Natural Resources Canada | Ressources naturelles Canada

GEOLOGICAL SURVEY OF CANADA
OPEN FILE 8385

The ups and downs of the Canadian Shield: 2 – preliminary results of apatite fission-track analysis from a 3.6 km vertical profile, LaRonde mine, Quebec

N. Pinet

2018

GEOLOGICAL SURVEY OF CANADA
OPEN FILE 8385

The ups and downs of the Canadian Shield: 2 – preliminary results of apatite fission-track analysis from a 3.6 km vertical profile, LaRonde mine, Quebec

N. Pinet

2018

Permanent link: https://doi.org/10.4095/308067

This publication is available for free download through GEOSCAN (http://geoscan.nrcan.gc.ca/).

Recommended citation
Pinet. N., 2018. The ups and downs of the Canadian Shield: 2 – preliminary results of apatite fission-track analysis from a 3.6 km vertical profile, the LaRonde mine, Quebec; Geological Survey of Canada, Open File 8385, 44 p. https://doi.org/10.4095/308067

Publications in this series have not been edited; they are released as submitted by the author.

The ups and downs of the Canadian Shield: 2 – preliminary results of apatite fission-track analysis from a 3.6 km vertical profile, LaRonde mine, Quebec

Nicolas Pinet [(1)]

[(1)] Natural Resources Canada, Geological Survey of Canada, 490 rue de la Couronne, Québec, Quebec, G1K 9A9

Abstract: The low-temperature (120-60°C) thermal history of eight samples from a 3.6 km vertical depth profile in the LaRonde Mine (Archean Abitibi greenstone belt, Quebec) has been investigated using apatite fission-track (AFT) analysis. All samples correspond to greywackes of the Cadillac Formation.

The AFT ages show a clear younging relationship with depth (increasing temperature), as expected for samples that maintained constant relative depths over time. Ages vary from 413 ± 51 Ma near the surface, to 148.5 ± 6.3 Ma for the deepest sample. Forward and inverse modeling indicate that a scenario with a constant temperature or minor heating during the Paleozoic better accounts for the fission track length distributions than a scenario with a constant cooling rate. These results support the possibility that the Abitibi region was covered by a sedimentary succession of moderate thickness during the Paleozoic.

1. Introduction

Apatite fission track (AFT) analysis is a geochronological method that constrains the thermal history at relatively low-temperatures (typically < 120°C). It has been proven very useful in geological settings that experienced significant vertical motions and/or marked changes in geothermal gradients over relatively short (1-100 Myr) period of time (Green and Duddy, 2012 and references herein).

In relatively stable continental interiors, the quantification of the low-temperature history using the AFT method is challenging due to very slow exhumation rates over very long periods of time (>> 100 Myr), low geothermal gradients and the possibility of a complex and polyphased geological history for which the sedimentary and magmatic records are often missing or only locally preserved.

This is the case of the Canadian Shield where several lines of evidence indicate that sedimentary units have been deposited during the Phanerozoic and subsequently eroded away from vast areas. However, the thickness, age and geographical distribution of such a paleo-sedimentary cover remain poorly constrained.

Here I report AFT data for eight samples from the LaRonde mine (Abitibi region, Quebec) and provide preliminary interpretations. This datasets complement AFT analysis from the Hudson Bay regions reported in Pinet et al. (2016) and in a companion paper (Pinet, in preparation). Another aim of this open file is to discuss modeling strategies and scenarios in more detail than it is usually possible in scientific journals.

2. Geological background

Due to its great depth (including a 2.2 km deep single-lift shaft) and to even deeper exploration holes (> 3.3 km), the LaRonde mine provides a unique opportunity to study a multi-kilometer vertical profile in which samples are expected to have kept a constant geometrical relationship since the last stages of regional deformation during the Precambrian.

The LaRonde Mine is located in the east-west-trending Doyon-Bousquet-LaRonde mining camp in the southern portion of the Archean Abitibi greenstone belt of the Abitibi region of northwest Quebec (Fig. 1; Mercier-Langevin et al., 2007). The mine has produced more than 5 million ounces of gold, as well as valuable by-products from massive and disseminated sulphide lenses within mafic and felsic volcanic rocks of the Bousquet Formation (Blake River Group) that form a steeply dipping, south facing homoclinal sequence. The volcanic host sequence of the LaRonde deposit is overlain to the south by sedimentary strata of the Cadillac Group that correspond to a turbiditic sequence younger than 2687 Ma.

From the LaRonde Mine, the nearest Paleozoic strata are those of the Lake Temiskaming outlier, which is located approximately 100 km to the SSW (Fig. 1).

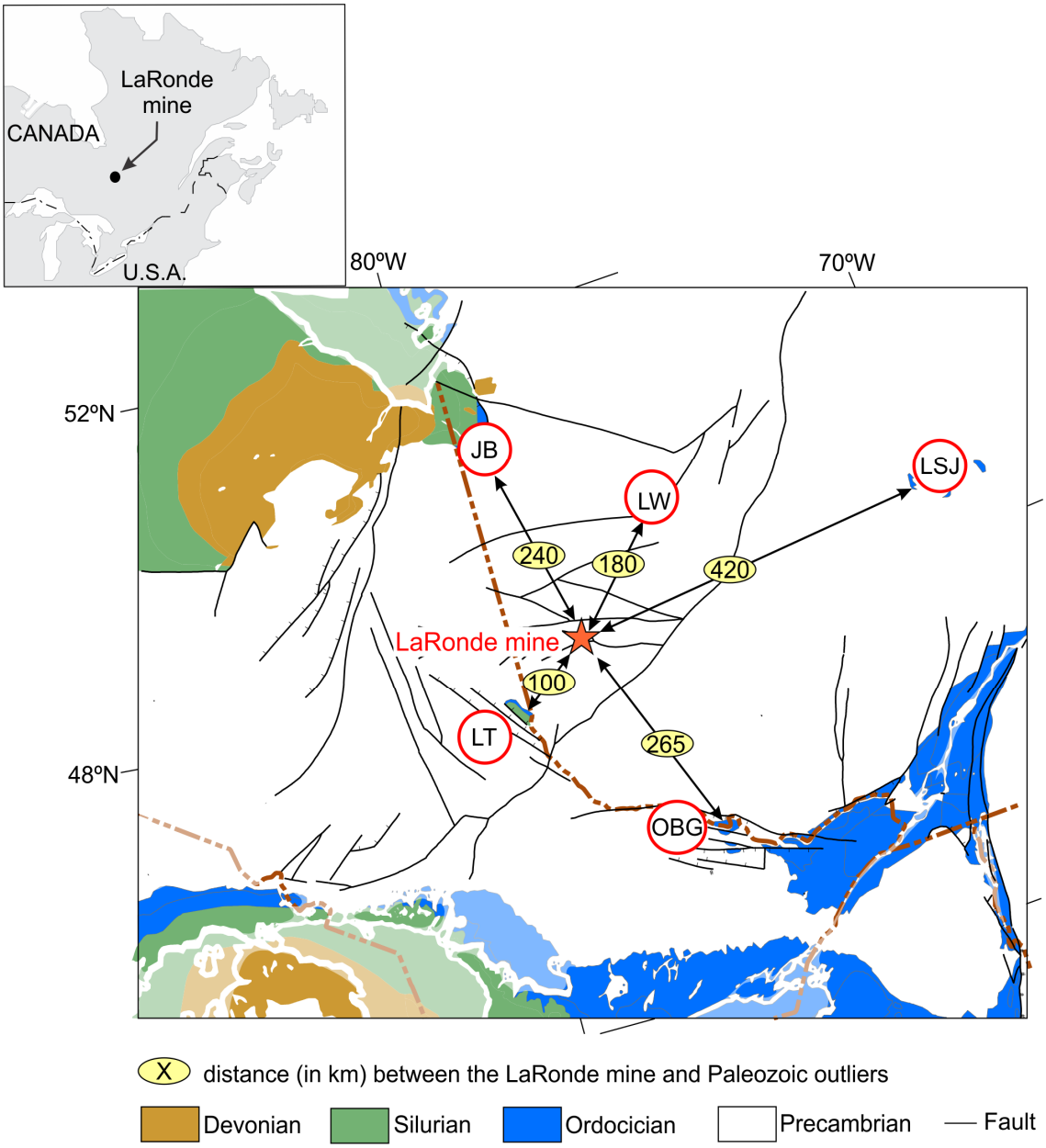

Figure 1: Location of the LaRonde mine showing the distances with Paleozoic outliers. JB, James Bay; LT, Lake Temiskaming; LSJ, Lake Saint Jean; LW, Lake Waswanipi; OBG, Ottawa-Bonnechère Graben;

3. Sampling strategy

Ten samples from greywackes of the Cadillac Group (Fig. 2) were sampled in several holes at elevation/depth varying between 317 and -3362 m. Among these samples, two did not contain enough apatite grains for AFT analysis.

Vertical intervals between samples discussed in this study vary between 288 m and 836 m (Table 1).

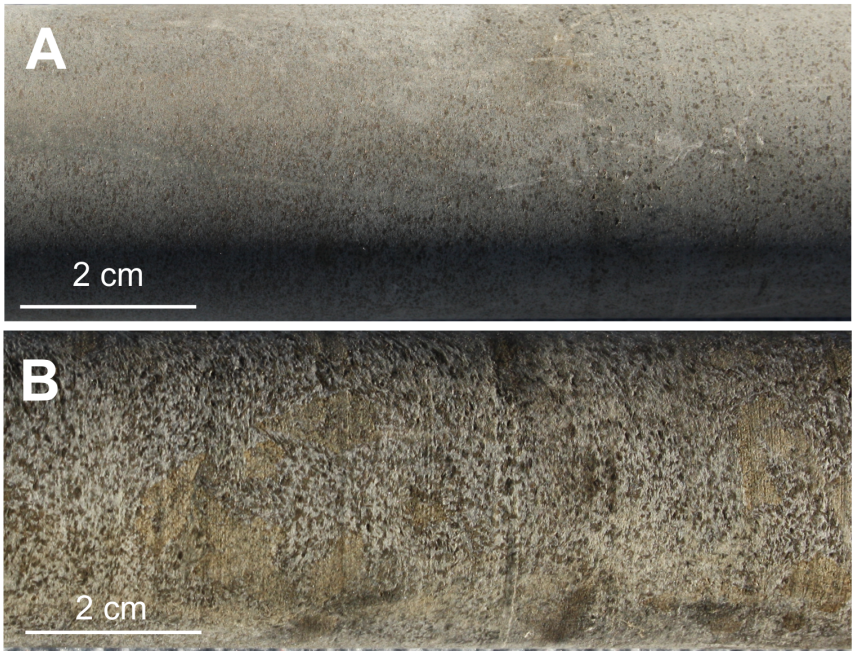

Figure 2: Greywacke of the Cadillac Group. A, sample CALRD145137; B, sample CALRD145141.

SAMPLE	HOLE	FROM	TO	COORDINATES UTM83-17			Unit
				Easting	Northing	Elevation (N.M.M)	
CALRD145132	106-01-07	14.6	16.1	692399.47	5347080.97	317.60	Greywacke, Cadillac Group
CALRD145133	106-00-06	629.5	631	693480.63	5347410.57	-147.52	Greywacke, Cadillac Group
CALRD145134	20-323	478.5	480	691940.22	5347044.50	-536.01	Greywacke, Cadillac Group
CALRD145135	20-333	684	685.5	692071.74	5347023.15	-983.64	Greywacke, Cadillac Group
CALRD145136	3086-11	930	931.5	692979.44	5347159.21	-1272.04	Greywacke, Cadillac Group
CALRD145137	3215-142	565.5	567	689409.10	5346751.27	-1769.33	Greywacke, Cadillac Group
CALRD145138	3218-60	792.5	794	691161.62	5346839.49	-2184.51	Greywacke, Cadillac Group
CALRD145139	3215-102	1119	1120.5	689535.97	5346545.46	-2602.89	Greywacke, Cadillac Group
CALRD145140	3215-103	1453.3	1454.8	689882.63	5346486.81	-2968.90	Greywacke, Cadillac Group
CALRD145141	LR-290-005	1092.8	1094.3	689891.29	5346353.45	-3361.99	Greywacke, Cadillac Group

Table 1: Summary of samples studied for AFT analysis. Grey shading indicate the samples with not enough apatites for AFT analysis (CALRD145134 and CALRD145138).

In the LaRonde mine area, the depth-temperature relationship has been determined using the higher temperatures measured with a Reflex EZ-Shot in exploration holes at depths comprised between 200 and 3400 m (David Pitre, personal communication).

The following relationship between in situ temperature (T, in °C) and depth (Y, in km) is used for mine planning:

$$T = 0.0012Y + 10$$

This relationship will be used during the modeling of AFT data.

4. The apatite fission track method

Apatite fission-track (AFT) analysis has been widely used during the past decades to constrain the low-temperature thermal histories of many areas around the world, in different geological settings. Isotopic dating methods are based on the ratio of parent and daughter isotopes, although for AFT analysis the daughter product is not another isotope but rather a trail of physical damage to the crystal lattice resulting from spontaneous fission of ^{238}U.

Fission tracks form at similar initial lengths continuously over time, at a rate dependent upon only uranium concentration. The fission tracks are shortened in the partial annealing zone (PAZ) that corresponds to temperatures between ~60°C and ~120°C (>200°C for the most 'retentive' apatite). At lower temperatures than the PAZ, fission tracks are still shortened but at much lower rates, whereas at higher temperatures, tracks are completely erased (annealed). During exhumation, earlier-formed tracks will tend to be shorter than later-formed ones, as they will have more time to anneal and may have experienced higher temperatures. The change in length of AFT varies among apatite crystals and two proxies are commonly used to estimate the kinetics of the annealing process: Dpar, which is a measure of the long axis of the etch pit opening (in µm) parallel to the crystallographic c-axis and the chlorine content (in weight %).

Interpretation of AFT data is based on the combined analysis of the fission track age, track length distribution and a kinetic parameter. Fission track ages do not usually indicate the timing of cooling through a specific temperature (except for nearly instantaneous cooling, such as in volcanic settings), but instead represent the integrated thermal history of studied samples. Excellent reviews on the AFT method are found in Gallagher et al. (1998), Gleadow et al. (2002), Donelick et al. (2005), Ketcham (2005) and Green and Duddy (2012).

5. Data

4a. Methodology

The AFT analyses reported here were conducted at Dalhousie University (Canada) using the external detector method.

All rock samples were broken into small pieces using a hydraulic splitter and jaw crusher, then ground in a disc mill and sieved to fragments <500 µm. The sieved material was then run over a Wifley mineral separation table to produce an initial heavy mineral concentrate, which was then treated with conventional magnetic and heavy liquid techniques to produce an apatite-bearing fraction.

Apatite aliquots were mounted in araldite epoxy on glass slides, ground and polished to an optical finish to expose internal grain surfaces. Polished mounts were etched in 5M HNO_3 for 20 seconds at 21°C to reveal the fossil tracks that intersect the polished apatite grain surface.

In the external detector method, the ^{238}U parent concentration is determined by using fission track density induced on a uranium free external detector (muscovite slab) from the fission of ^{235}U through irradiation with a flux of slow thermal neutrons (see Donelick et al., 2005 for details). Samples and CN5 glass standards were irradiated with thermal neutrons. After irradiation, the low-U muscovite detectors that covered apatite grain mounts and glass dosimeter were etched in 5.5 N HNO_3 for 20 s at 21˚C to reveal induced fission tracks.

Samples were analysed using a Kinetek computer-controlled stage driven by the FTSage software attached to a Zeiss Axioplan microscope.

4b. Results

Apatite fission track (AFT) results for eight samples from the LaRonde mine area are summarized in Tables 2 and 3.

For the four deepest samples (CALRD145137 to CALRD145141), the age determination is based on 20-22 apatite grains per sample and track length data include 32 to 62 measurements. For three of the shallowest samples (CALRD145132, CALRD145133 and CALRD145136), the AFT age is based on 19-20 grains per sample, but confined track length data are restricted to 0-4 measurements, making these later useless. It should be noted that the Uranium content of the three shallowest samples is very low (Table 2), which translates to higher uncertainties. Only 7 apatite grains were analyzed for sample CALRD145135, and the calculated AFT age has a high uncertainty and is considered unreliable (see below).

Sample	Elevation / Depth (m)	No of grains	ρs (10^6 cm^{-2})	Ns	ρi (10^6 cm^{-2})	Ni	ρd (10^6 cm^{-2})	Nd	P(χ^2) (%)	Central Age ± 1σ (Ma)	U (ppm)
CALRD145132	317.6	15	0.406	217	0.178	95	1.03	5269	91.9	4.37 ± 52	2.47
CALRD145133	-147.2	19	0.793	284	0.444	159	1.04	5269	80.4	9.67 ± 33	6.4
CALRD145135	-983.6	5	0.053	5	0.096	9	1.07	5269	83.5	5.47 ± 59	1.2
CALRD145136	-1272.0	19	1.022	255	0.849	212	1.10	5269	47.9	5.16 ± 22	10.62
CALRD145137	-1769.3	22	0.741	784	0.679	718	1.11	5269	70.9	5.90 ± 12	11.35
CALRD145139	-2602.9	20	3.016	918	3.449	1050	1.14	5269	15.4	7.66 ± 10	40.4
CALRD145140	-2968.9	20	2.516	1514	3.133	1885	1.17	5269	10.7	1.22 ± 8.	39.73
CALRD145141	-3362.0	21	1.557	934	2.256	1353	1.20	5269	88.0	7.91 ± 7.	25.57

LEGEND

Zeta	362.7
Zeta error	7.8
Decay k	1.55 E-10
RhoD	(varies for each sample)
ND	5269
Area	8.985065 E-7 cm^2
Ns	number of spontaneous tracks counted
ρs	density of spontaneous tracks
Ni	number of induced tracks counted
ρi	density of induced tracks on mica
Nd	number of tracks counted in the dosimetry glass
ρd	density of tracks on dosimetry glass
X^2 test	(P > 5%) is a pass on the X^2 test
U	average U concentration (ppm) of grains used for age calculation

Table 2: AFT age results for eight samples from the LaRonde mine area. Central age, calculated from single grain ages after Galbraith (2005).

Sample	Elevation / Depth (m)	Confined Track-Lengths (TL)	MTL µm ± 1σ	MTL Std dev µm	Dpars µm	Dpar error µm	Cl wt% (mean)	Cl wt% (min)	Cl wt% (max)
CALRD145132	317.6	4	11.64 ± 0.37	0.73	2.38	1.03	0.002	0.000	0.011
CALRD145133	-147.2	2	13.24 ± 0.27	0.39	2.28	0.99	0.010	0.003	0.066
CALRD145135	-983.6	0	--	-	2.16	1.05	0.018	0.003	0.031
CALRD145136	-1272.0	3	10.45 ± 0.97	1.67	2.5	1.05	0.016	0.000	0.032
CALRD145137	-1769.3	48	11.65 ± 0.27	1.87	2.39	0.98	0.008	0.000	0.027
CALRD145139	-2602.9	32	10.05 ± 0.56	3.18	2.56	1.06	0.003	0.000	0.019
CALRD145140	-2968.9	54	10.22 ± 0.33	2.44	2.57	1.03	0.026	0.000	0.289
CALRD145141	-3362.0	62	10.31 ± 0.31	2.47	2.49	1.05	0.019	0.001	0.240

LEGEND

MTL	Mean Track Length (c-axis not corrected)
Dpar	four Dpar measurements were averaged from each analysed crystal when available;

Table 3: AFT track length results and kinetic parameters (D_{par} and Cl wt%) for eight samples from the LaRonde mine area. D_{par} corresponds to the etch pit diameter. Cl wt% clearly demonstrate the predominance of fluorapatite.

The chi-square (χ^2) test calculated for each sample analysed (Table 2) is a standard test for the homogeneity of single grain ages. It provides an assessment of whether the fission track counts were derived from a Poissonian distribution with a common mean value. If the χ^2-statistic $P(\chi^2)$ is ≥ 5%, (as is the case for all samples discussed here) it can be taken as evidence that all grains counted derive from a single age population.

All samples exhibit narrow etch pits (Table 3), suggesting that the predominant composition of the grains analysed is fluorapatite. This was confirmed by electron microprobe analyses of apatites (Fig. 3). Average Cl wt% of apatite on which AFT ages were determined ranges from 0.002 to 0.026% (maximum single grain apatite Cl wt% = 0.289). Apatite grains with such low values of Cl wt% usually anneal more readily relative to those with higher Cl wt% (> 1-2%), (Donelick et al., 2005).

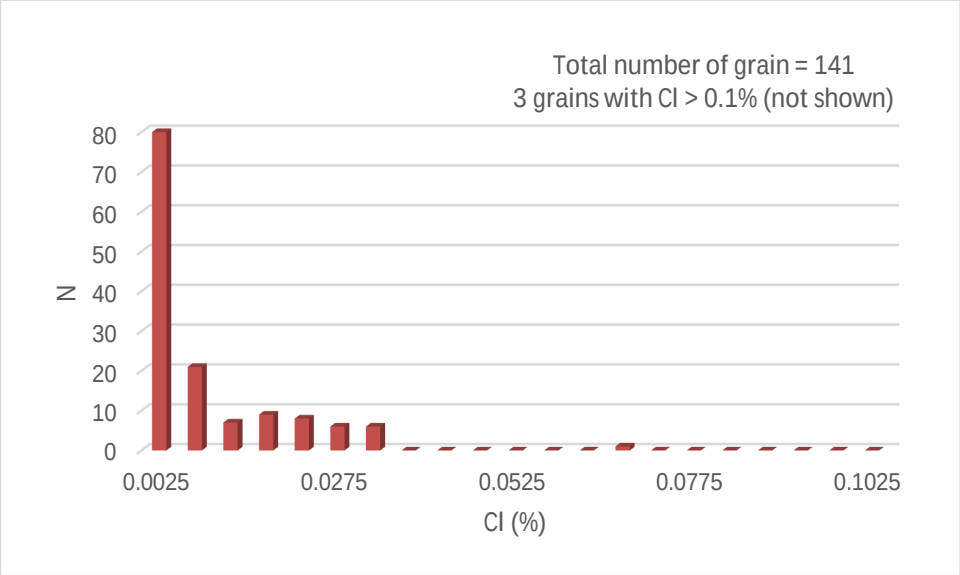

Figure 3: Chlorine content (in %) of apatite grains from the LaRonde Mine.

Samples yield AFT pooled ages ranging from 413 ± 51 to 148.5 ± 6.3 Ma. As expected for samples that preserved their geometrical position one compared to the other, a clear relationship exists between the AFT age and the elevation (Fig. 4), the deepest sample yielding the youngest age. A notable exception to this relationship is sample CALRD145135, but as noted above its AFT age is considered as poorly reliable.

Interestingly, the AFT age – elevation relationship does not correspond to a single straight line (Fig. 4). This characteristic will be discussed later.

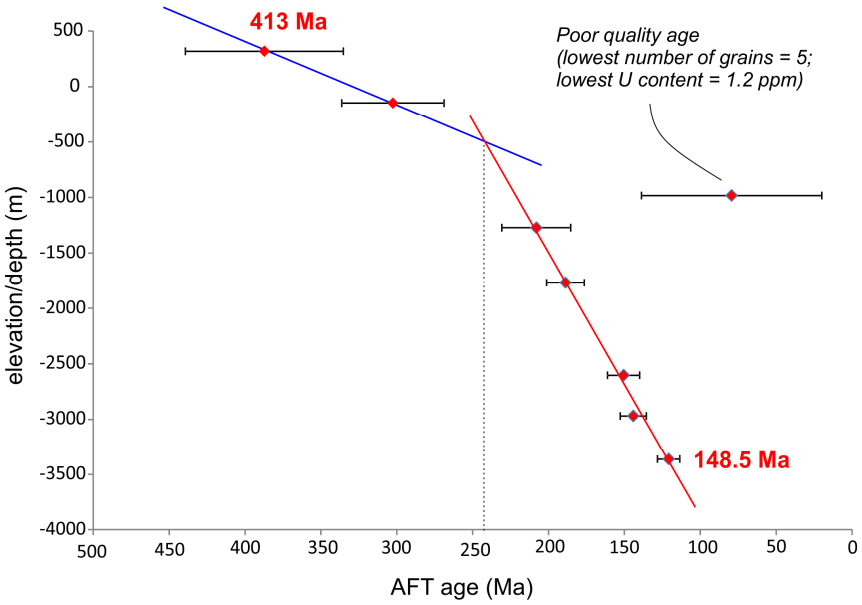

Figure 4: AFT age versus elevation relationship for samples from the LaRonde Mine.

Mean horizontal confined track lengths for the 4 samples with >30 length data range from 10.05 ± 0.56 to 11.65 ± 0.27 μm (Table 3). Among these samples, the shallowest (depth= -1769.33 m) has a mean track length significantly greater (11.65 ± 0.27 μm) than the other three samples (10.05 ± 0.56 to 10.31 ± 0.31 μm) located 853.6 m to 1593.7 m below it.

6. Modeling strategy

6a. Forward modeling

Forward model in which the AFT age and track length distribution are calculated from a given T-t history is a useful preliminary interpretation tool in areas, such the LaRonde mine, for which geological constraints on the low-temperature history are lacking.

Figure 5 shows the results of forward models of a slow and continuous decrease of temperature over time. These models indicates that the present-day temperature and AFT age of samples can be honoured if paleo-temperatures were between 150˚C and 270˚C at 1 Ga.

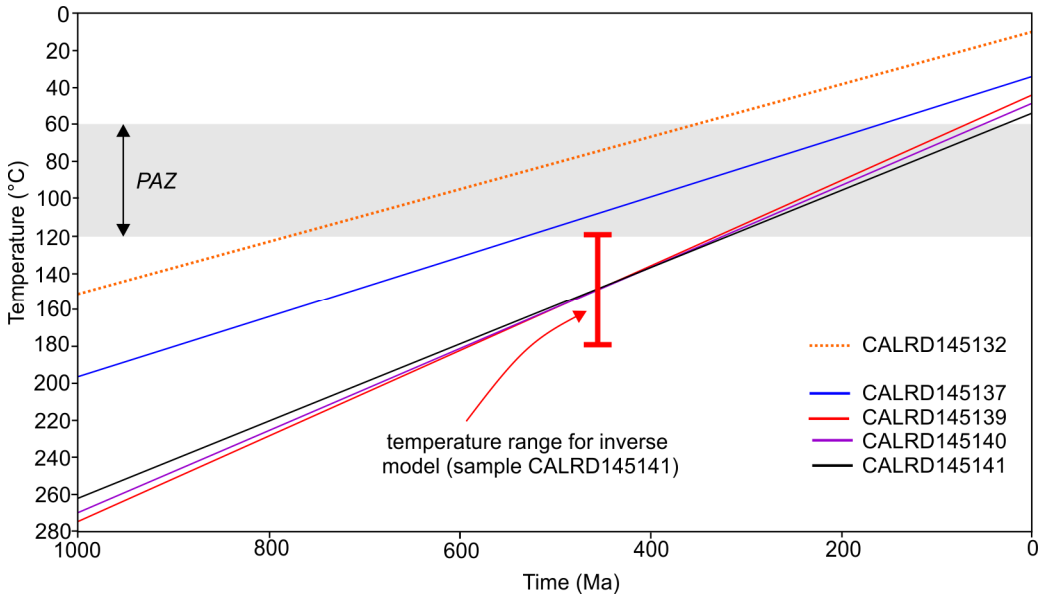

Figure 5: T-t histories with a slow and continuous decrease in temperature that account for both the AFT age and the present-day temperature. PAZ is the partial annealing zone.

Results of such forward models (Table 4) also indicate that the low-temperature histories do not account well for length data (goodness of fit between 0 and 0.44 for samples with more than 30 measurements). The calculated mean track length is shorter than the measured track length, which suggests that the residence time in the partial annealing zone in a slow-continuous cooling model is too short (or too simplistic).

	Model Pooled age	Measured pooled age	Model track length	Measured track length	GOF
CALRD45141	149	149	12.99 +/- 1.24	12.54 +/- 1.17	0.10
CALRD45140	168	168	13.18 +/- 1.26	11.99 +/- 1.65	0.00
CALRD45139	178	178	13.29 +/-1.28	12.55 +/- 1.45	0.24
CALRD45137	216	216	13.15 +/- 1.23	13.15 +/- 1.26	0.44

Table 4: Results of forward models testing a slow and continuous decrease of temperature over time (Fig. 5). Note the poor goodness of fit (GOF) for length data.

One way to reconcile the measured and predicted track length data is to allow an increase in temperatures during the Paleozoic, a scenario in agreement with subsidence analysis and thermal maturity studies in the Hudson Bay Basin and AFT results within and around the basin (Pinet et al., 2013 and 2016; Lavoie et al., 2015). This scenario will be tested during inverse modeling.

6b. Basic parameters used during inverse modeling

A number of software tools that use several approaches to invert fission track data for modeling thermal histories are available. Modeling strategies and applications are discussed in Issler (1996), Willet (1997), Ketcham (2005), Donelick et al. (2005), Ehlers et al. (2005), Gallagher (2012), Ketcham (2013), Vermeesch and Tian (2014) and Gallagher and Ketcham (2018) amongst others.

In this study, AFT ages, track lengths and Dpar measurements were used to determine T-t paths using inverse Monte Carlo modeling (HeFTy software, version 1.8.2; Ketcham, 2013; modified from Ketcham, 2005). The Ketcham et al. (2007) multi-compositional annealing model was used, with *c*-axis projected track length data. The Dpar kinetic parameter was used to calibrate annealing kinetics and an initial confined track length (calculated according the formula of Carlson et al., 1999). The standard length reduction is 0.893 in all models. For the analysis reported here, the Zeta factor (a parameter determined by calibration with international standards of known ages) is: 362.7 ± 7.8.

HeFTy also allows the user to specify regions of time-temperature (T-t) space through which each path must pass. The additional division of path segments between user-defined T-t boxes can also introduce complexity to the thermal history. In HeFTy, the complexity of T-t paths is taken into account by three main parameters:

1) The number of times (n) a path segment between two constraints is halved by introducing a new point allowing a change in slope (2^n segments between constraints). Increasing the number of nodes allows a greater complexity to the model.
2) A qualitative measure of the possible changes in the T-t path with three modes: 'episodic' in which sudden changes are allowed, 'intermediate' which is less prone to sudden changes and 'gradual' where the temperature changes gradually over time.
3) A maximal heating/cooling rate for each segment.

The choice of these parameters depends on the tectonic setting and on geological knowledge. Considering the intracratonic setting of the Hudson Bay region, rapid temperature changes are unlikely (Pinet et al., 2016). For this reason, in all inverse models presented the maximal heating/cooling rate has been set to be lower or equal to 2°C/My and the changes in the T-t path have been qualified as 'intermediate'.

The goodness of fit for each thermal history was assessed using Kuiper's Statistic. Good fit and acceptable fit paths have goodness-of-fit values of > 0.75 and 0.05, respectively. The best way to consider the paths is that a 'good' fit implies that the T-t path is *supported* by the data, while an acceptable T-t path is *not ruled out* by the data (Ketcham, 2013). Further, the HeFTy software highlights a "best fit" path (shown as a heavy black line) for modelling runs as well as predicted AFT ages and track length

information for that path, which can be readily compared with the measured parameters. Although the best-fit path most closely matches the measured parameters it is emphasized that other T-t paths (especially good fit paths) are also possible.

For all inverse models presented in this study, the Monte Carlo modeling ended when 100 good paths had been generated.

7. Inverse modeling results for sample CALRD145141

As noted previously, only a few confined track lengths were measured on the four shallowest samples, which makes the inversion less constrained.

Among the three deepest samples, sample CALRD45141 shows the highest $P(\chi^2)$ probability, lowest AFT age uncertainty and the greatest number of measured track lengths. It is thus considered as the most 'robust' sample and will be used as the reference sample for modelling. Once completed for sample CALRD45141, the same inverse modeling strategy will be apply to other samples taking into account the fact that they maintained a fixed relationship (depth interval) during the last billion years.

Sample CALRD45141 yielded a central AFT age of 148.5 ± 6.3 Ma.

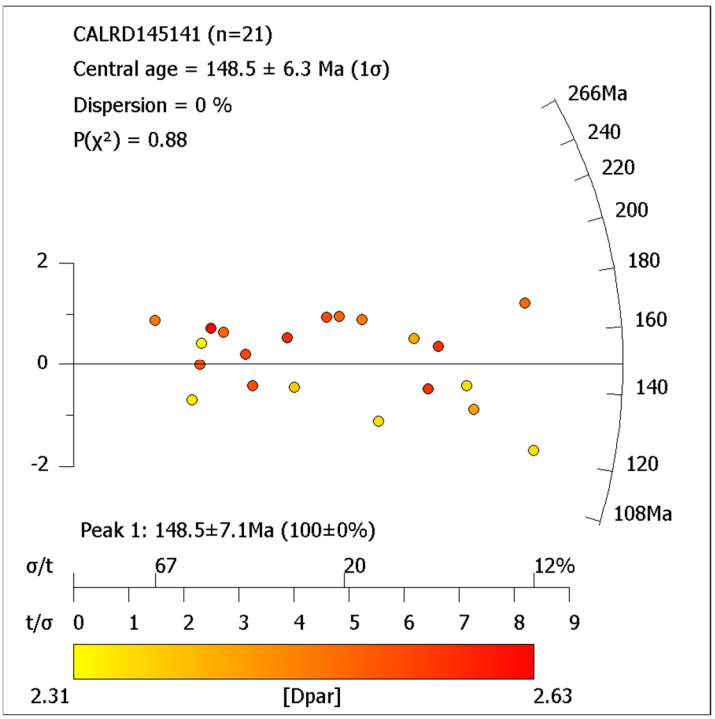

Figure 6: Radial plot for sample CALRD45141. On this diagram, more precise fission track ages plot further from the origin along the x-axis (precision). Radial plot done using the RadialPlotter software (Vermeesch, 2009).

The mean track length (non-projected) is 10.31 ± 0.31 µm. C-axis projected horizontal track lengths range between 10.17 and 14.81 µm and show a unimodal distribution.

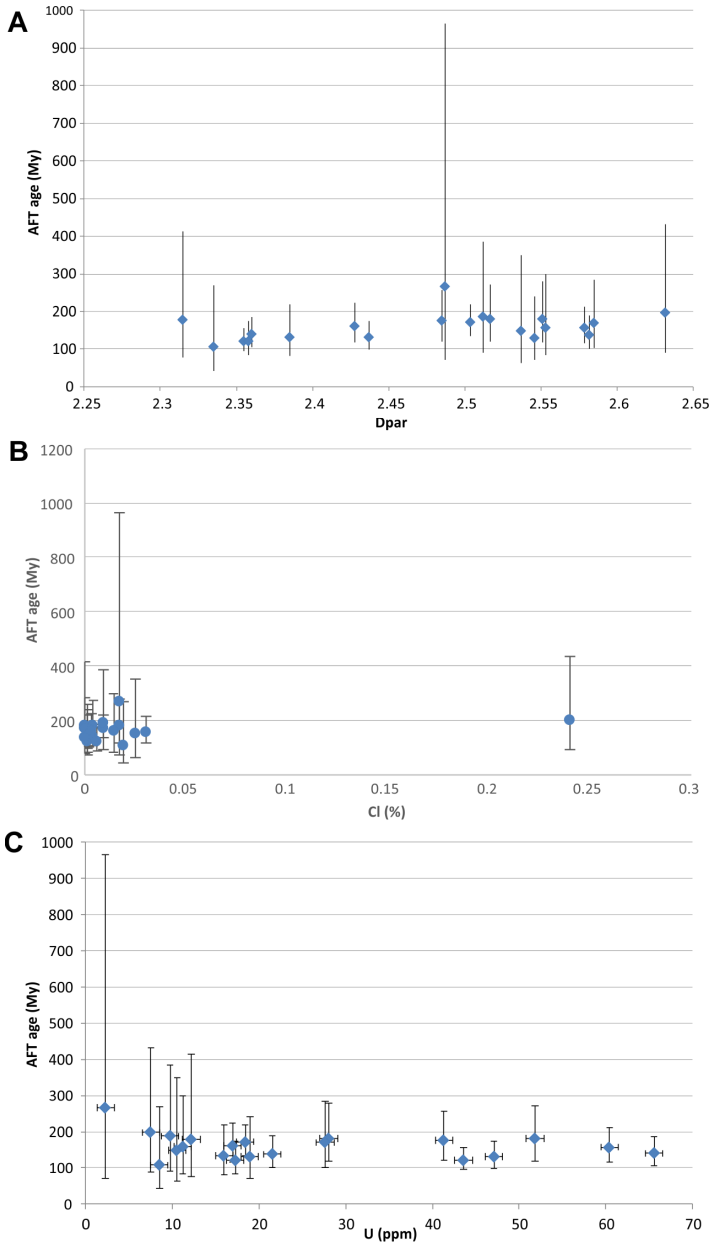

Figure 7: Diagrams showing (A) Dpar versus age; (B) Cl (%) versus age; and (C) Uranium content versus age for sample CALRD45141.

Mean Dpar values (average of four measurements by crystals when available) range from 2.315 to 2.632 µm, with an average of 2.49 µm. No relationship exists between AFT age and Dpar (Fig. 7A) suggesting that the annealing kinetics of single grains in the sample are homogeneous. All apatite grains analysed have chlorine content ≤ 0.3%, except one

that yielded 0.24 % (Figure 7B). No obvious relationship exists between the uranium content and the AFT age (Figure 7C).

A temperature of 150˚C ± 30˚C at 450-400 Ma (Fig. 8A and 8C) is used as a constraint during inverse modelling. The temperature estimate is based on forward models of slow and constant decrease in temperature that account for both the age and present-day temperature (but not length data; Fig. 5). The timeframe (Late Ordovician-Early Devonian) corresponds to the most probable period for initial sedimentary burial (if any) based on regional considerations (Pinet et al., 2013; Lavoie et al., 2015).

A period of constant temperature or heating due to sediment deposition is loosely defined for the period 425-350 Ma (mid-Silurian to Early Carboniferous). This constraints aims to test the possibility of burial by Paleozoic sediments.

Finally, the present-day temperature is used as a constraint for inverse modelling.

Modeling results indicates that both the AFT age (goodness of fit = 0.98) and the track length distribution (goodness of fit = 0.95) can be adequately fit with such scenario. However, the changes in temperatures (and indirectly the thickness of a potential sedimentary cover) are not well constrained as good fit paths exhibit considerable scattering. On Figure 8, the best fit model exhibits a clear increase (± 40˚C), but the weighted mean path shows a period of almost constant temperature between 450 and 360 Ma. The inverse models results also shows a change in the cooling rate at around 230 Ma. This last point will be discussed later.

An alternative model in which the temperature at 450-400 Ma is more loosely constraint (± 50˚C of the estimate based on the slow and constant decrease in temperature forward model, instead of 30˚C) is presented on Figure 8D. In this case, both the best fit path and mean weighted path exhibit a nearly constant temperature between 450 and 375 Ma.

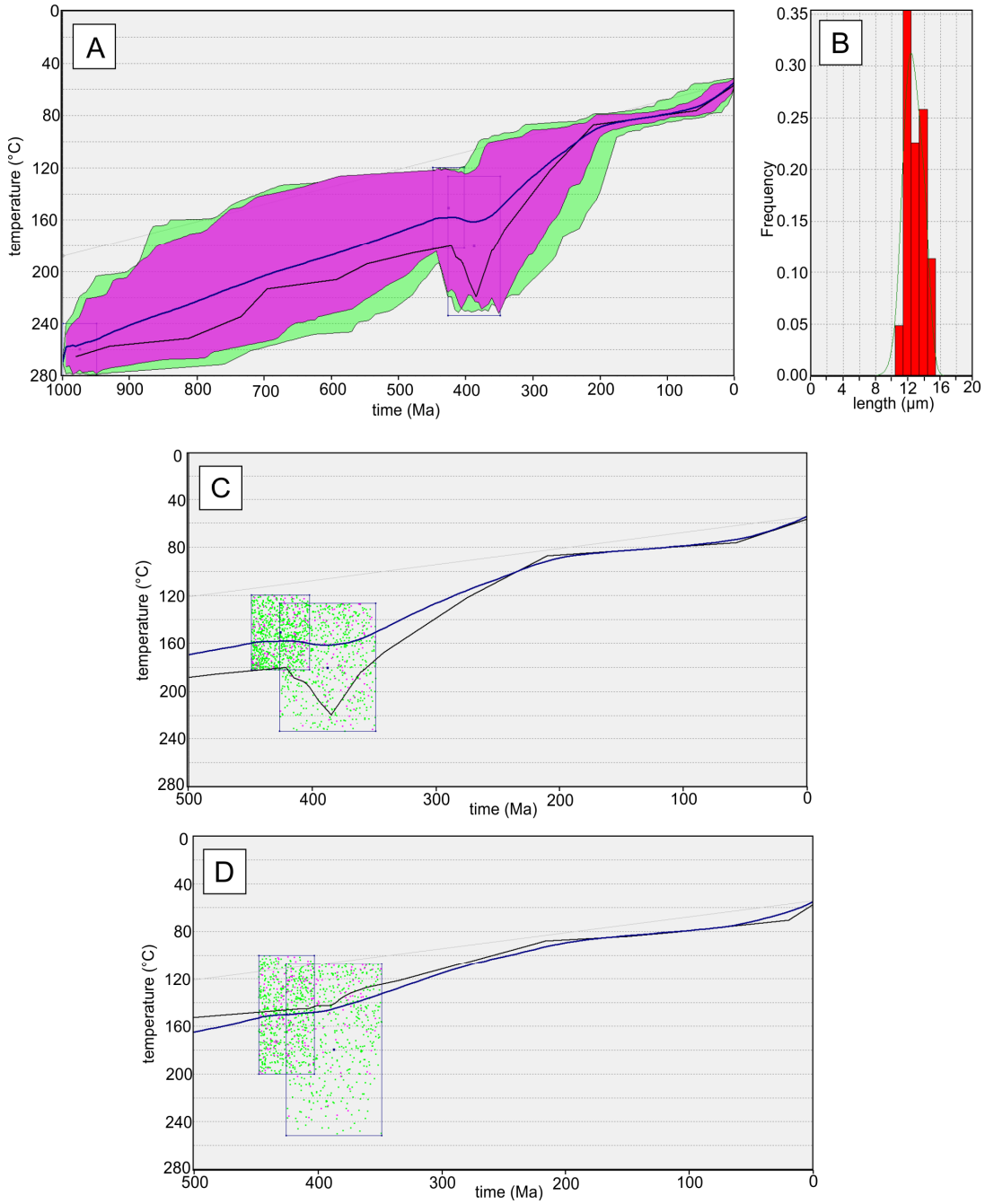

Figure 8: Inverse model results for sample CALRD145141. A) Envelopes including all the good paths (magenta) and acceptable paths (green). The best fit path is shown as a black line and the weighted mean path as a blue line. B) Track length distribution. The green curve is the calculated distribution. C) Plot of peak heating points within each of the T-t constraint boxes. D) Plot of peak heating points within each of the T-t constraint boxes for an alternative model with more loosely defined constraints. In C) and D) Good points are magenta, acceptable are green. Note the change of horizontal scale compared to (A).

Inverse modelling using the same T-t constraints as the base model, but Cl (%) as the kinetic parameter is shown in Figure 9. Results are quite similar, except that the goodness of fit for length is lower (0.82). A model (not shown) excluding the highest Cl (%) value (0.24%) gives almost identical results

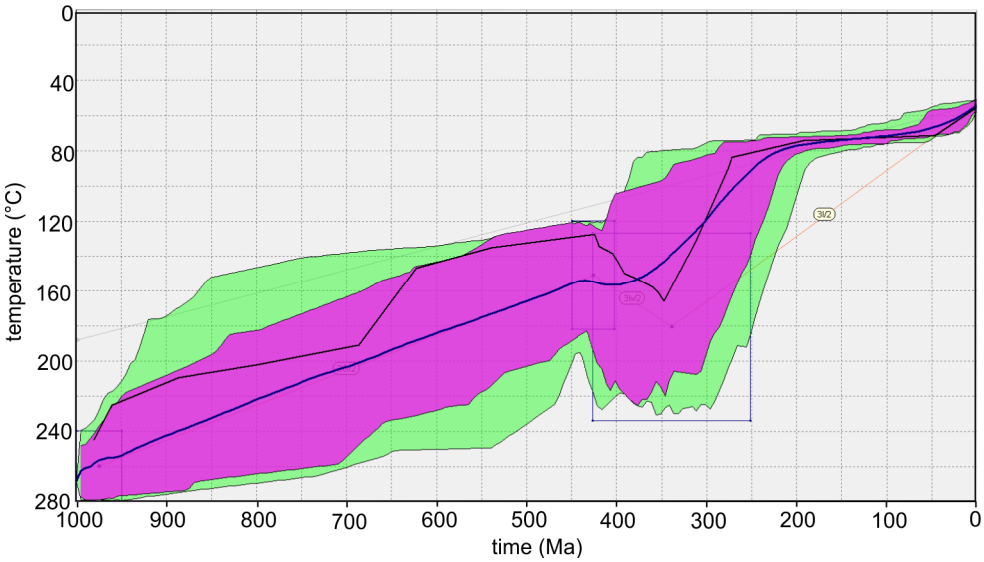

Figure 9: Inverse model results for sample CALRD145141 using Cl (%) as the kinetic parameter. Envelopes including all the good paths (magenta) and acceptable paths (green). The best fit path is shown as a black line and the weighted mean path as a blue line.

8. Inverse modeling of samples CALRD145132 to CALRD145140

Taking advantage of the vertical distribution of samples, the T-t constraints were applied to the other samples with track data, by considering that the difference in temperature between samples was constant over time (Table 5).

sample	depth (m)	depth difference (m)	temperature difference (°C)	temperature 1Ga (°C)		temperature 450 Ma (°C)		present-day temperature
141	3362			262	±20	150	±30	54
140	2969	393	5	257	±20	145	±30	49
139	2603	759	9	253	±20	141	±30	45
137	1769	1,593	19	243	±20	131	±30	35
136	1272	2,090	25	237	±20	125	±30	29
135	983.6	2,378	29	233	±20	121	±30	26
133	147.5	3,215	39	223	±20	111	±30	16
132	-317.6	3,680	44	218	±20	106	±30	10

Table 5: Summary of constraints used for the inverse modelling of samples from the LaRonde mine.

Inverse modelling provides good T-t paths honouring the constraints for all the samples. For samples with track length data (CALRD145137 to CALRD145140), the goodness of fit for AFT age vary between 0.97 and 1.00. The goodness of fit for length data is 0.99 (sample CALRD145137), 0.92 (sample CALRD145139) and 0.74 (sample CALRD145140).

All the mean weighted T-t paths show a three stages evolution (Figure 10): 1) a period of almost constant temperature (except for the shallowest sample) centered around 425 Ma. This period is partly controlled by the imposed constraints; 2) a period of significant cooling; 3) a period of slow decrease of temperature between 200 and 300 Ma.

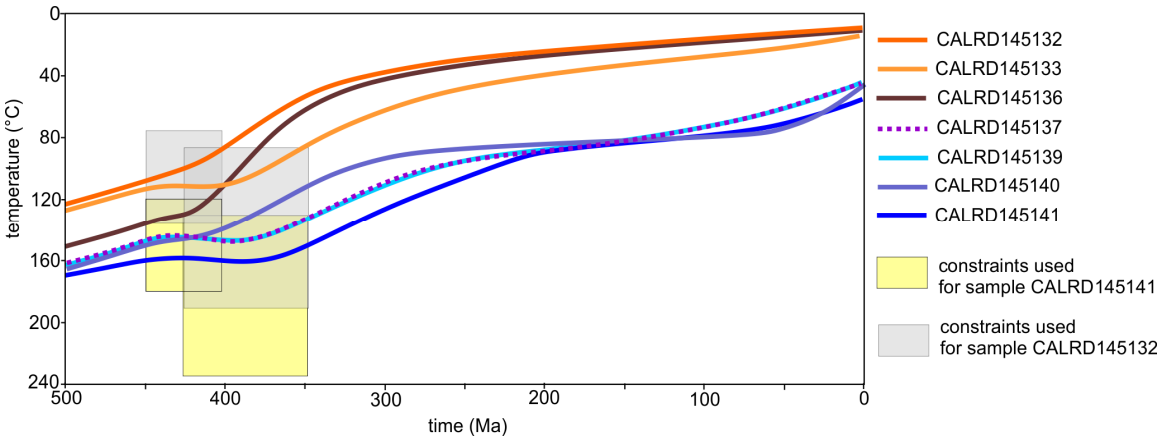

Figure 10: Weighted mean T-t path for the seven samples of the LaRonde mine that have been modelled.

The fact that all of the mean weighted T-t paths exhibit a quite similar shape demonstrates that the tested thermal scenario in which there is no cooling or even a slight increase in temperature during the Paleozoic is a viable hypothesis for the entire dataset.

9. Discussion

Inverse models for all the seven samples studied indicated that a scenario involving an increase or a constant temperature during the Ordovician-Carboniferous period better explains the data than constant cooling during this period (higher goodness of fit for AFT length data). This suggests that the possibility of a thin Paleozoic sedimentary cover over the Abitibi region is a viable scenario. However, it should be acknowledged that the lack of direct geological constraints in the Abitibi region for the last billion years prevents a more accurate analysis and other T-t scenarios may possibly honours as well individual data.

Another way to look at the data is to exploit the spatial relationship of samples and to analyse the results collectively. In particular, the fact that the AFT age-elevation relationship (AER) does not correspond to a single straight line (Fig. 4) is noteworthy. In geological terms, the change in the slope of the AER indicates that the cooling rate

decreases after 250 Ma, a change already suggested by the mean weighted paths of inverse models (Fig. 10).

In low-temperature thermochronology studies, a change in the slope of the AFT age-elevation curve has been traditionally interpreted as either due to a change in thermal gradient or a change in the denudation rate. The insulating effects of low-conductivity rocks such as mudstone and basalts on the underlying rocks (Luszczak et al., 2017) are probably not significant for a low thermal gradient region and the variations of surface temperature, even if important for low-temperature thermochronology interpretations, are not expected to be abrupt. Alternatively, the change in the slope of the AER may results from radiation enhanced annealing at sub-PAZ temperatures. Such interpretation, first proposed by Hendriks and Redfield (2005), was partly based on an age-elevation relationship for two wells located in Finland that shows a similar shape than the one defined in the LaRonde mine. These authors noted that the uranium concentration and AFT age (with depth) were highly correlated and suggested that low temperature annealing would be amplified in higher eU apatites by the thermal histories in cratonic settings. However, as noted by Green and Duddy, 'the concept of 'radiation-enhanced annealing' currently finds little support outside its direct proponents'.

In the Abitibi region, a sharp change in the thermal gradient during the Paleozoic seems improbable as no local magmatic activity occurred during that time.

A decrease of denudation rate at ca. 250 Ma could be related to the far-field effects of a drastic change of geodynamic setting on the eastern side of Laurentia, i.e. the transition from an active margin characterized by mountain building to a passive margin, after the Alleghanian orogeny. Alternatively, a decrease in denudation rate can be related to the effects of rock erodibility variations. These effects have been recently quantified by Flowers and Elhers (2018) who demonstrated that the exhumation of soft sedimentary rocks overlying crystalline basement causes earlier cooling and thus older thermochronometric ages, as well as a change in cooling rate due to the change in erodibility. This effect should be apparent in an intracratonic setting where dramatic changes in denudation rates are not expected.

The mechanism explaining a decrease of denudation rate can be tested through a regional approach. The external erosional forcing hypothesis implies a continental-scale event and the change of geodynamic setting should be recorded in existing regional low-temperature thermochronologic data. On the contrary, the timing of the cooling rate deceleration may change in the rock erodibility hypothesis, depending on the thickness of the (easily removed) sedimentary cover. Testing these hypothesis will be the aim of future works.

10. Summary and Perspective

The low-temperature (60-120°C) thermal history of eight samples from a 3.6 vertical profile in the LaRonde mine has been investigated using apatite fission track (AFT) analysis. These samples correspond to Archean greywackes of the Cadillac Group. Seven samples yielded reliable ages between 413 ± 51 and 148.5 ± 6.3 Ma.

Inverse modeling results suggest that a scenario involving a period of constant temperature or low heating during the Ordovician-Carboniferous period more adequately explains the data than a minor, constant decrease in temperature during this period (higher goodness of fit for length data). The hypothesis of a deposition of a thin cover of Paleozoic sediments is thus viable, even if still unproven.

The AFT age-elevation diagram shows a cooling rate deceleration around 260 Ma. This change is also suggested by inverse models of individual samples and can be interpreted as a change in thermal gradient (less likely), a change in denudation rate (related to the change of geodynamic setting on the eastern side of Laurentia?) or a change in rock erodibility (preferred). This last hypothesis would support the presence of a thin Paleozoic sedimentary cover eroding at faster rates than Archean basement.

At the regional scale, more data are needed to resolve the thermal history of the Canadian Shield, to decipher regional trends, and constrain the timing of maximum heating. Additional samples from the LaRonde Mine area, and especially from the near surface and at ± 600 m depth (AER break in the slope) would put additional constraints in the low-temperature history of the Abitibi region.

8. Acknowledgments

David Pitre is thanked for providing the samples. Without his help, this study would not have been possible. Thanks also to Denis Lavoie for his support during the GEM program and Kalin McDannell (GSC-Calgary) for the internal review of the manuscript.

9. References

Carlson, W.D. Donelick, R.A. and Ketcham, R.A., 1999. Variability of apatite fission-track annealing kinetics: I. Experimental results. American Mineralogist, 84, 1213-1223.

Donelick, R.A., O'Sullivan, P.B., Ketcham, R.A., 2005. Apatite fission track analysis. Reviews in Mineralogy and Geochemistry, 58, 49-94.

Ehlers, T.A., Chaudhri, T., Kumar, S., Fuller, C.W., Willet, S., Ketcham, R.A., Brandon, M.T., Belton, D.X., Kohn, B.P., Gleadow, A.J.W., Dunai, T.J., Fu, F.Q., 2005. Computational tools for low-temperature thermochronometer interpretation. Review in Mineralogy & Geochemistry, 58, 589-622.

Flowers, R.M., Ehlers, T.A., 2018. Rock erodibility and the interpretation of low-temperature thermochronologic data. Earth and Planetary Science Letters, 482, 312-323.

Galbraith, R.F. 2005. *Statistics for fission track analysis*. Chapman & Hall/CRC, Boca Raton, USA, 219

Gallagher, K., 2012. Transdimensional inverse thermal history modeling for quantitative thermochronology. Journal of Geophysical Research, 117, B02408.

Gallagher, K., Brown, R., Johnson, C., 1998. Fission track analysis and its applications to geological problems. Annual Review Earth and Planetary Sciences, 26, 519-572.

Gallagher, K., Ketcham, R.A., 2018. Comment on 'Thermal history modelling: HeFTy vs QTQt' by Vermeesch and Tian. Earth Science Reviews, 176, 387-394.

Gleadow, A.J.W., Belton, D.X., Kohn, B.P., Brown, R.W., 2002. Fission track dating of phosphate minerals and the thermochronology of apatite. *In* Kohn, M., Rakovan, J. and Hugues, J.M. (eds.) Phosphates – Geochemical, Geobiological and Material importance, Reviews in Mineralogy and Geochemistry, 48, 579-630.

Green, P.F., Duddy, I.R., 2012. Thermal history reconstruction in sedimentary basins using apatite fission-track analysis and related techniques. *In*: Analysing the thermal history of sedimentary basins: method and case studies, SEPM Special Publication No 103, p. 65-104.

Hendriks, B.W.H, Redfield, T.F., 2005. Apatite fission track and (U-Th)/He data from Fennoscandia: an example of underestimation of fission track annealing in apatite. Earth and Planetary Science Letters, 236, 443-458.

Issler, D.R., 1996. An inverse model for extracting thermal histories from apatite fission-track data: instruction and software for Window 95 environment. Geological Survey of Canada, Open File 2325, 84 p.

Ketcham, R.A., 2005. Forward and inverse modeling of low-temperature thermochronometry data. Review in Mineralogy and Geochemistry, 58, 275-314.

Ketcham, R.A. Carter, A. Donelick, R.A. Barbarand, J. and Hurford, A.J. 2007. Improved modeling of fission-track annealing in apatite. American Mineralogist, 92, 799–810.

Ketcham, R.A., 2013. HeFTy, version 1.8.2. Manual user dated 2 october 2013.

Lavoie, D., Pinet, N., Dietrich, J., Chen, Z., 2015. The Paleozoic Hudson Bay Basin in northern Canada: new insights into hydrocarbon potential of a frontier intracratonic basin: American Association of Petroleum Geologist Bulletin, 99, 859-888.

Luszczak, K., Persano, C., Braun, J., Stuart, F., 2017. How local crustal thermal properties influence the amount of denudation derived from low-temperature thermochonometry. Geology, 45, 779-782.

Mercier-Langevin, P., Dubé, B., Hannington, M.D., Davis, D.W., Lafrance, B., Gosselin, G., 2007. The LaRonde Penna Au-rich volcanogenic massive sulfide deposit, Abitibi greenstone belt, Quebec: Part I. Geology and geochronology. Economic Geology, 102, 585-609.

Pinet, N., Lavoie, D., Dietrich, J., Hu, K., Keating, P., 2013. Architecture and subsidence history of the Hudson Bay intracratonic basin. Earth-Science Review, 125, 1-23.

Pinet, N., Kohn, B.P., Lavoie, D., 2016. The ups and dows of the Canadian Shield: 1-preliminary results of apatite fission track analysis from the Hudson Bay region. Geological Survey of Canada, Open File 8110, 59 p.

Vermeesch, P., 2009. RadialPlotter: a Java application for fission track, luminescence and other radial plots. Radiation Measurements, 44, 4, 409-410.

Vermeesch, P., Tian, Y., 2014. Thermal history modelling: HeFTy vs. QTQt. Earth Science Reviews, 139, 279-290.

Willet, S.D., 1997. Inverse modeling of annealing of fission tracks in apatite - 1: a controlled random search method. American Journal of Science, 297, 939-969

ANNEX: AFT RESULTS

SAMPLE: CALRD145132

Age: Archean
Geological unit: Cadillac Group
Type: Greywacke

Coordinates - UTM83-17
Easting 692399.47
Northing 5347080.97
Elevation
(N.M.M.) 317.60

present-day tempe 10˚C

GRAIN DATA

Number of grains	15
Number of Dpars	59

Grain#	Ns	Ni	# square	MDpar	MDprp	U (ppm)
1	29	14	50	2.631	1.111	4
2	6	2	50	2.393	0.989	1
3	6	1	40	2.447	0.998	0
4	7	2	70	2.07	1.089	0
5	5	2	24	2.123	1.213	1
6	3	1	35	1.847	1.03	0
7	3	1	30	2.261	1.183	0
8	49	17	16	2.417	0.9	15
9	10	3	18	2.081	0.932	2
10	78	44	63	2.052	0.965	10
11	4	1	72	2.591	1.187	0
12	8	2	12	2.19	0.791	2
13	7	3	70	2.202	1.109	1
14	0	1	30	2.267	1.021	0
15	2	1	15	2.204	1.083	1

LENGTH_DATA

Number_of_lens	4
Number_of_dpar	12

#	Len	Type	MDpar	MDprp	NDpar	Angle with C-axis
1	12.295	T	2.656	1.082	4	68.072
2	12.209	T	2.656	1.082	0	56.046
3	10.828	T	2.527	0.997	4	29.519
4	11.208	T	2.267	1.021	4	40.544

MICROPROBE DATA

MASS PERCENT

Grain No.	P2O5	La2O3	F	SiO2	Cl	CaO	Ce2O3	Na2O	SrO	FeO	MnO	Total
1	41.338	0.041	3.423	0.034	0.007	54.113	0.220	0.033	0.000	0.040	0.052	97.858
2	41.749	0.032	3.163	0.000	0.000	54.426	0.021	0.000	0.000	0.000	0.034	98.093
3	41.850	0.000	3.599	0.000	0.001	55.134	0.000	0.015	0.000	0.000	0.043	99.127
4	41.492	0.000	3.289	0.000	0.001	53.854	0.000	0.000	0.000	0.019	0.056	97.326
5	42.289	0.000	4.120	0.000	0.011	54.722	0.031	0.040	0.000	0.065	0.082	99.623
6	42.735	0.111	3.560	0.000	0.001	54.139	0.029	0.037	0.000	0.006	0.062	99.181
7	42.200	0.027	3.289	0.000	0.003	55.072	0.032	0.026	0.000	0.041	0.048	99.352
8	42.109	0.021	3.947	0.000	0.000	54.445	0.011	0.053	0.000	0.004	0.028	98.956
9	42.081	0.016	3.417	0.103	0.000	54.355	0.213	0.065	0.000	0.016	0.037	98.864
10	41.818	0.103	3.355	0.001	0.000	53.831	0.246	0.074	0.000	0.049	0.040	98.104
11	41.714	0.000	3.391	0.000	0.000	53.927	0.000	0.008	0.000	0.016	0.042	97.670
12	41.531	0.096	3.331	0.012	0.002	54.104	0.157	0.086	0.000	0.003	0.082	98.001
13	41.720	0.000	3.314	0.000	0.001	54.110	0.000	0.004	0.000	0.000	0.055	97.809
14	41.868	0.000	3.421	0.000	0.002	55.575	0.034	0.032	0.000	0.000	0.022	99.514
15	42.325	0.148	3.143	0.000	0.000	55.338	0.008	0.024	0.000	0.001	0.076	99.740

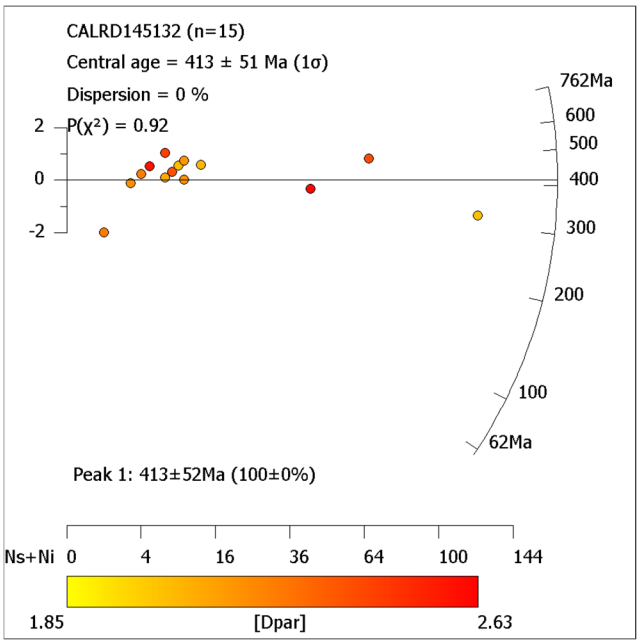

SAMPLE: CALRD145133

Age: Archean
Geological unit: Cadillac Group
Type: Greywacke

Coordinates - UTM83-17

Easting	693480.63
Northing	5347410.57
Elevation (N.M.M.)	-147.52

present-day temper 16˚C

GRAIN DATA

Number of grains	20
Number of Dpars	77

Grain#	Ns	Ni	# square	MDpar	MDprp	U (ppm)
1	15	5	30	2.366	0.926	2
2	39	14	25	2.558	1.158	8
3	4	5	20	2.515	0.941	3
4	28	15	12	2.562	1.086	17
5	8	3	25	2.519	1.096	2
6	8	2	27	2.016	0.912	1
7	1	1	8	2.282	0.995	2
8	12	12	6	2.247	0.991	28
9	2	1	15	2.254	0.856	1
10	4	1	15	2.096	0.919	1
11	4	3	16	2.02	0.841	3
12	4	4	25	1.895	0.886	2
13	6	4	56	2.376	1.006	1
14	16	7	24	2.166	1.089	4
15	25	12	16	2.591	0.879	10
16	3	3	15	1.355	0.931	3
17	4	1	10	2.196	1.135	1
18	85	58	30	2.613	1.119	27
19	16	8	24	2.618	0.836	5

LENGTH_DATA

Number_of_lens	2
Number_of_dpar	8

#	Len	Type	MDpar	MDprp	NDpar	Angle with C-axis
1	12.965	T	2.19	0.976	4	83.974
2	13.511	T	2.361	1.02	4	64.451

MICROPROBE DATA

MASS PERCENT

Grain No.	P2O5	La2O3	F	SiO2	Cl	CaO	Ce2O3	Na2O	SrO	FeO	MnO	Total
1	41.839	0.059	3.424	0.000	0.005	54.520	0.084	0.019	0.000	0.009	0.031	98.547
2	42.032	0.000	3.047	0.000	0.008	54.018	0.025	0.061	0.000	0.034	0.069	98.009
3	42.276	0.122	3.304	0.000	0.003	55.186	0.000	0.000	0.000	0.019	0.002	99.520
4	41.849	0.000	3.264	0.000	0.004	54.260	0.005	0.035	0.000	0.012	0.081	98.135
5	41.360	0.000	2.990	0.000	0.003	54.348	0.102	0.060	0.000	0.161	0.050	97.814
6	41.590	0.000	3.501	0.000	0.066	54.954	0.013	0.000	0.000	0.008	0.041	98.684
7	41.885	0.000	3.419	0.000	0.002	54.492	0.005	0.039	0.000	0.014	0.057	98.473
8	42.224	0.000	3.604	0.000	0.010	55.223	0.023	0.046	0.000	0.006	0.049	99.666
9	42.124	0.000	3.322	0.000	0.004	54.864	0.015	0.005	0.000	0.020	0.056	99.010
10	41.517	0.018	3.505	0.000	0.003	54.703	0.000	0.030	0.000	0.000	0.068	98.367
11	42.339	0.000	3.868	0.000	0.004	55.234	0.028	0.017	0.000	0.032	0.089	99.981
12	42.648	0.000	3.670	0.000	0.023	55.096	0.056	0.031	0.000	0.029	0.052	100.055
13	41.920	0.000	2.897	0.000	0.009	54.795	0.048	0.000	0.000	0.000	0.077	98.524
14	42.291	0.000	3.558	0.000	0.021	54.946	0.000	0.033	0.000	0.000	0.044	99.390
15	41.716	0.022	3.442	0.000	0.004	54.154	0.025	0.022	0.000	0.028	0.035	97.998
16	42.486	0.000	3.554	0.000	0.010	54.955	0.043	0.011	0.000	0.014	0.090	99.665
17	42.041	0.000	2.952	0.000	0.003	54.134	0.066	0.000	0.000	0.051	0.071	98.074
18	41.442	0.096	3.216	0.113	0.003	53.335	0.475	0.055	0.000	0.005	0.000	97.385
19	41.911	0.044	3.336	0.000	0.005	55.091	0.028	0.040	0.000	0.035	0.070	99.154

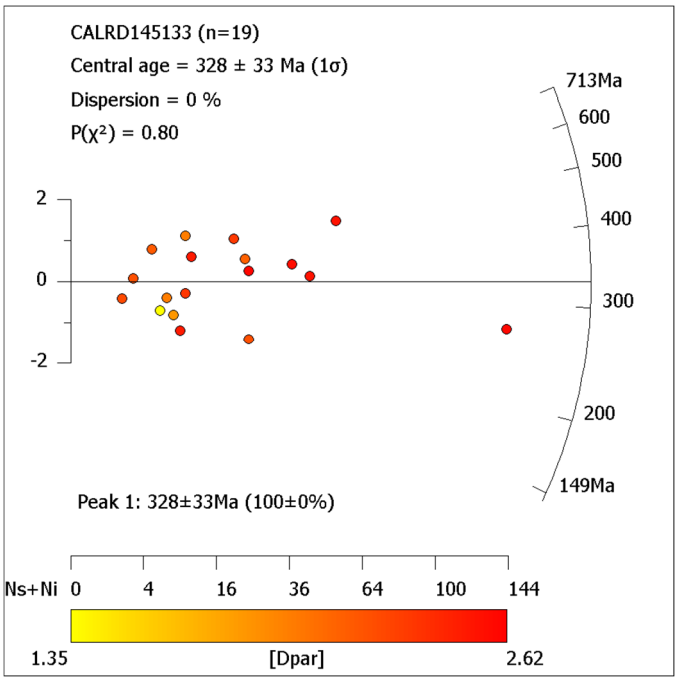

SAMPLE: CALRD145135

Age: Archean
Geological unit: Cadillac Group
Type: Greywacke

Coordinates - UTM83-17

Easting	692071.74
Northing	5347023.15
Elevation (N.M.M.)	-983.64

present-day temperature 26˚C

GRAIN_DATA

Number of grains	5
Number of Dpars	13

Grain#	Ns	Ni	# square	MDpar	MDprp	U (ppm)
1	1	1	10	2.568	1.323	1
2	0	1	24	1.565	1.107	1
3	3	4	35	2.227	0.94	2
4	1	2	24	2.489	1.154	1
5	0	1	12	0	0	1

LENGTH_DATA

Number_of_lens	0
Number_of_dpar	0

MICROPROBE DATA

MASS PERCENT

No.	P2O5	La2O3	F	SiO2	Cl	CaO	Ce2O3	Na2O	SrO	FeO	MnO	Total
1	42.382	0.031	3.764	0.000	0.021	54.642	0.000	0.000	0.000	0.022	0.086	99.358
2	42.266	0.000	4.020	0.000	0.016	54.836	0.000	0.011	0.000	0.000	0.058	99.510
3	41.689	0.000	4.019	0.000	0.019	55.352	0.053	0.009	0.000	0.009	0.059	99.513
4	42.130	0.000	3.633	0.000	0.031	54.230	0.086	0.000	0.000	0.051	0.058	98.682
5	42.541	0.000	4.054	0.000	0.003	54.714	0.000	0.019	0.000	0.022	0.073	99.718

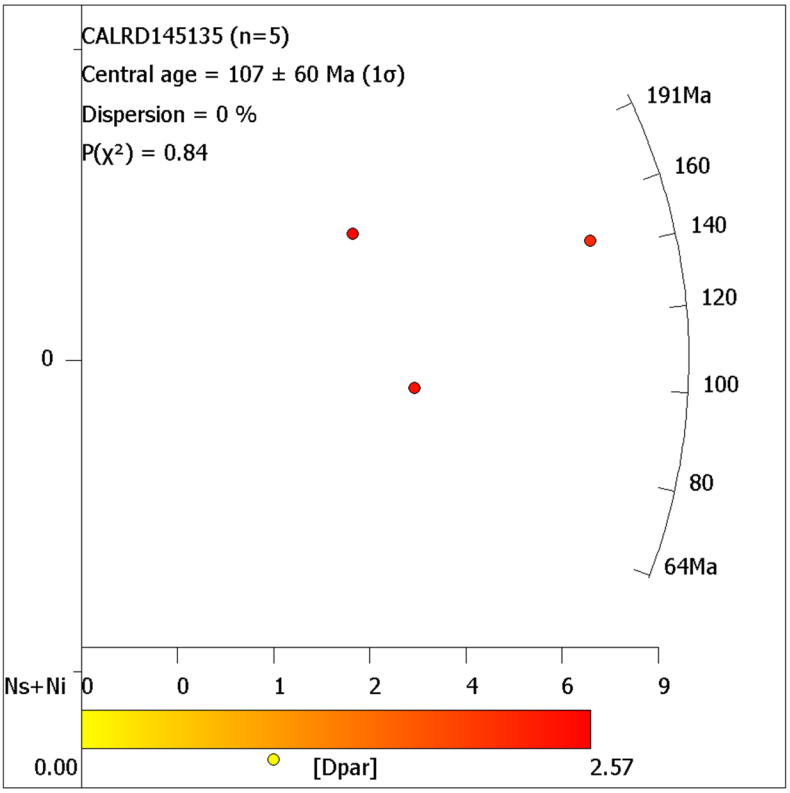
CALRD145135 (n=5)
Central age = 107 ± 60 Ma (1σ)
Dispersion = 0 %
P(χ²) = 0.84
191Ma
160
140
120
100
80
64Ma
0
Ns+Ni
0
0
1
2
4
6
9
0.00
[Dpar]
2.57

SAMPLE: CALRD145136

Age: Archean
Geological unit: Cadillac Group
Type: Greywacke

Coordinates - UTM83-17

Easting	692979.44
Northing	5347159.21
Elevation (N.M.M.)	-1272.04

present-day temperature 29˚C

GRAIN_DATA

Number of grains	19
Number of Dpars	76

Grain#	Ns	Ni	# square	MDpar	MDprp	U (ppm)
1	20	15	8	2.57	1.045	25
2	7	4	8	2.691	1.122	7
3	9	7	16	2.535	1.005	6
4	12	3	12	2.478	1.108	3
5	6	6	24	2.255	1.156	3
6	5	3	12	2.572	0.923	3
7	2	3	12	2.07	1.078	3
8	15	13	10	1.988	1.025	17
9	13	15	20	2.673	1.088	10
10	4	7	18	2.429	0.914	5
11	7	2	8	2.475	1.211	3
12	12	12	6	2.492	0.992	27
13	24	15	20	2.481	1.052	10
14	28	28	24	2.706	0.96	15
15	26	11	20	2.539	1.113	7
16	6	4	8	2.637	1.074	7
17	2	3	20	2.035	1.431	2
18	46	45	20	2.878	1.075	30
19	11	16	12	2.545	1.039	18

LENGTH_DATA

Number_of_lens	3
Number_of_dpar	12

#	Len	Type	MDpar	MDprp	NDpar	Angle with C-axis
1	8.731	T	2.679	0.936	4	82.916
2	10.532	T	2.436	1.035	4	52.772
3	12.075	T	2.481	1.091	4	64.877

MICROPROBE DATA

MASS PERCENT

Grain No.	P2O5	La2O3	F	SiO2	Cl	CaO	Ce2O3	Na2O	SrO	FeO	MnO	Total
1	40.610	1.905	2.957	0.092	0.009	48.109	4.462	0.019	0.000	0.004	0.000	96.920
2	41.654	0.000	3.416	0.000	0.031	54.593	0.127	0.027	0.000	0.152	0.037	98.592
3	42.179	0.068	3.823	0.000	0.010	54.747	0.124	0.042	0.000	0.001	0.080	99.462
4	42.214	0.000	3.662	0.000	0.029	54.781	0.041	0.070	0.000	0.181	0.082	99.511
5	42.316	0.045	3.663	0.000	0.021	54.923	0.135	0.010	0.000	0.057	0.055	99.678
6	42.207	0.000	3.871	0.000	0.002	54.732	0.094	0.073	0.000	0.093	0.151	99.593
7	42.770	0.104	3.639	0.000	0.007	54.740	0.036	0.067	0.000	0.107	0.098	100.034
8	41.801	0.075	3.556	0.000	0.018	54.665	0.074	0.024	0.000	0.049	0.042	98.803
9	42.244	0.027	3.383	0.000	0.007	54.672	0.033	0.066	0.000	0.109	0.065	99.180
10	41.595	0.023	3.959	0.006	0.015	54.933	0.135	0.056	0.000	0.119	0.086	99.257
11	42.321	0.000	3.326	0.000	0.020	55.012	0.028	0.063	0.000	0.075	0.114	99.554
12	42.286	0.000	4.113	0.000	0.030	54.775	0.000	0.059	0.000	0.015	0.060	99.599
13	41.958	0.013	3.638	0.000	0.019	54.807	0.096	0.028	0.000	0.007	0.038	99.068
14	41.704	0.000	3.907	0.000	0.013	54.891	0.096	0.033	0.000	0.104	0.044	99.144
15	42.582	0.018	3.669	0.000	0.004	54.698	0.104	0.058	0.000	0.103	0.142	99.832
16	41.809	0.017	3.377	0.030	0.032	54.148	0.018	0.061	0.000	0.140	0.048	98.251
17	42.844	0.000	3.906	0.000	0.000	54.884	0.053	0.040	0.000	0.085	0.036	100.203
18	41.875	0.000	3.324	0.000	0.009	54.685	0.066	0.029	0.000	0.029	0.106	98.721
19	41.754	0.007	3.493	0.000	0.029	54.597	0.069	0.034	0.000	0.050	0.051	98.606

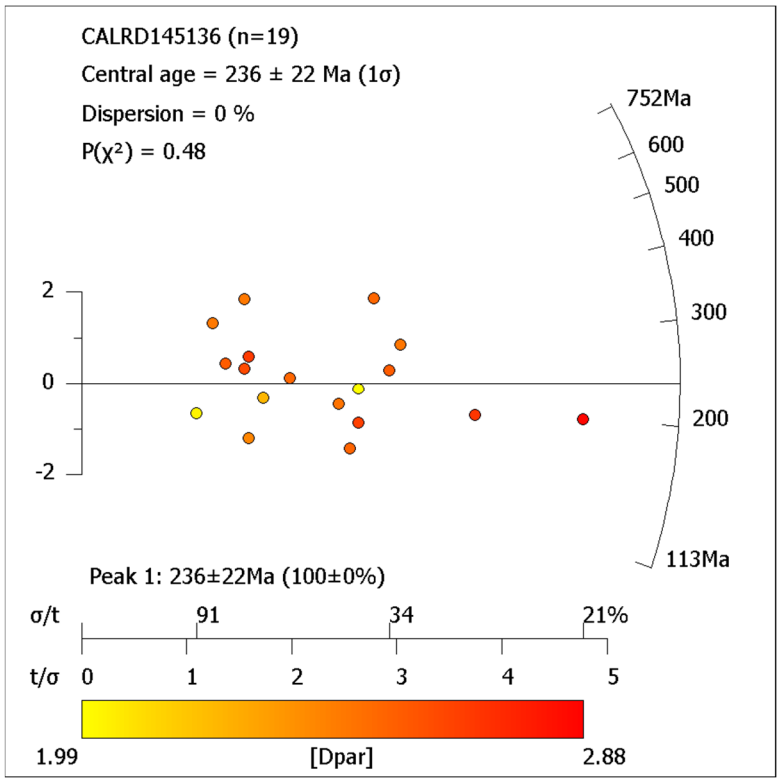

SAMPLE: CALRD145137

Age: Archean
Geological unit: Cadillac Group
Type: Greywacke

Coordinates - UTM83-17

Easting	689409.10
Northing	5346751.27
Elevation (N.M.M.)	-1769.33

present-day temperature 35˚C

GRAIN_DATA

Number of grains	22
Number of Dpars	88

Grain#	Ns	Ni	# square	MDpar	MDprp	U (ppm)
1	42	35	18	2.429	0.939	26
2	49	47	56	2.415	1.002	11
3	7	8	100	2.259	0.944	1
4	3	3	54	2.313	0.937	1
5	134	111	40	2.566	1.137	36
6	33	34	30	2.447	1.083	15
7	3	5	36	2.394	1.186	2
8	18	12	72	2.297	0.956	2
9	9	11	100	2.45	0.997	1
10	15	8	100	2.258	0.84	1
11	63	79	100	2.248	0.938	10
12	81	57	42	2.495	0.924	18
13	81	66	70	2.117	0.848	12
14	20	12	56	2.206	0.824	3
15	9	14	40	2.228	0.961	5
16	35	30	63	2.184	1.034	6
17	5	5	50	2.152	1.167	1
18	17	24	18	2.552	0.903	18
19	6	4	60	2.314	1.03	1
20	14	11	24	2.326	0.957	6
21	42	43	21	2.404	1.025	27
22	98	99	28	2.332	1.04	46

LENGTH_DATA

Number_of_lens	48
Number_of_dpar	104

#	Len	Type	MDpar	MDprp	NDpar	Angle with C-axis
1	10.448	T	2.451	0.946	4	55.204
2	11.883	T	2.451	0.946	0	56.327
3	11.353	T	2.514	0.95	4	59.064
4	11.165	T	2.514	0.95	0	77.948
5	12.036	T	2.514	0.95	0	71.243
6	12.544	T	2.514	0.95	0	66.371
7	14.532	T	2.514	0.95	0	40.742
8	8.898	T	2.514	0.95	0	42.661
9	14.008	T	2.415	0.924	4	74.905
10	10.153	T	2.628	0.907	4	55.505
11	13.355	T	2.628	0.907	0	33.269
12	11.275	T	2.895	0.999	4	47.511
13	14.24	T	2.277	1.016	4	47.653
14	9.97	T	2.154	0.977	4	75.787
15	11.58	T	2.329	0.905	4	46.72
16	9.425	T	2.459	0.88	4	73.294
17	12.667	T	2.459	0.88	0	66.658
18	9.93	T	2.459	0.88	0	64.446
19	12.013	T	2.459	0.88	0	57.383
20	12.409	T	2.28	0.88	4	60.327
21	12.701	T	2.229	0.889	4	61.455
22	11.572	T	2.229	0.889	0	86.586
23	13.706	T	1.978	0.852	4	59.447
24	13.177	T	2.361	0.915	4	55.962
25	12.801	T	2.531	0.861	4	65.48
26	10.724	T	2.622	0.869	4	56.86
27	14.012	T	2.622	0.869	0	73.457
28	12.224	T	2.374	0.977	4	31.035
29	12.283	T	2.604	1.039	4	73.062
30	12.394	T	2.534	1.248	4	69.919
31	5.951	T	2.674	0.838	4	59.838
32	9.485	T	2.638	1.088	4	73.18
33	13.525	T	2.638	1.088	0	76.42
34	9.546	T	2.638	1.088	0	33.249
35	10.441	T	2.638	1.088	0	46.813
36	9.584	T	2.323	1.005	4	84.327
37	8.021	T	2.323	1.005	0	48.148
38	12.82	T	2.323	1.005	0	65.258
39	9.036	T	2.323	1.005	0	67.773
40	11.459	T	2.323	1.005	0	70.849
41	12.672	T	2.303	0.973	4	66.197
42	14.485	T	2.307	1.096	4	81.655
43	9.889	T	2.409	1.023	4	47.469
44	11.966	T	2.409	1.023	0	52.493
45	14.18	T	2.497	0.901	4	50.151
46	10.309	T	2.301	1.075	4	55.657
47	12.54	T	2.301	1.075	0	52.409
48	13.982	T	2.301	1.075	0	79.999

TRACK_LENGTH_SUMMARY

Number	0	48	0	48	0	0
Mean_Len	-1	11.654	-1	11.654	-1	-1
SE_Mean	0	0.27	0	0.27	0	0
SD_Dist	0	1.870	0	1.870	0	0
Skewness	0	-0.631	0	-0.631	0	0
Kurtosis	0	0.403	0	0.403	0	0

MICROPROBE DATA

MASS PERCENT

Grain No.	P2O5	La2O3	F	SiO2	Cl	CaO	Ce2O3	Na2O	SrO	FeO	MnO	Total
1	40.840	0.047	3.741	0.000	0.027	54.966	0.005	0.032	0.000	0.050	0.128	98.255
2	40.977	0.000	3.647	0.000	0.000	54.464	0.061	0.027	0.000	0.029	0.114	97.783
3	41.365	0.000	3.493	0.000	0.003	54.600	0.005	0.000	0.000	0.052	0.121	98.167
4	40.940	0.029	3.172	0.000	0.027	54.743	0.000	0.018	0.000	0.052	0.192	97.831
5	40.610	0.027	3.755	0.000	0.000	54.471	0.010	0.049	0.000	0.231	0.110	97.682
6	41.659	0.000	3.770	0.000	0.001	54.471	0.135	0.019	0.000	0.026	0.103	98.597
7	40.812	0.067	3.281	0.000	0.023	54.284	0.000	0.047	0.000	0.052	0.129	97.309
8	40.805	0.000	3.036	0.000	0.026	54.746	0.000	0.022	0.000	0.067	0.168	97.586
9	40.859	0.002	3.474	0.000	0.009	54.337	0.000	0.000	0.000	0.102	0.173	97.491
10	40.990	0.008	3.787	0.000	0.003	54.531	0.000	0.000	0.000	0.052	0.134	97.909
11	40.435	0.012	3.410	0.020	0.001	54.470	0.157	0.022	0.000	0.104	0.091	97.286
12	41.094	0.025	3.580	0.000	0.008	55.049	0.046	0.037	0.000	0.041	0.110	98.481
13	41.264	0.010	3.460	0.000	0.004	54.708	0.000	0.023	0.000	0.100	0.110	98.221
14	40.540	0.101	3.482	0.000	0.013	54.212	0.000	0.024	0.000	0.013	0.097	97.013
15	40.227	0.031	3.768	0.000	0.000	54.664	0.000	0.014	0.000	0.000	0.108	97.225
16	40.273	0.003	3.630	0.000	0.001	54.482	0.043	0.029	0.000	0.212	0.092	97.237
17	40.783	0.000	3.069	0.000	0.006	54.695	0.020	0.043	0.000	0.000	0.209	97.532
18	40.369	0.077	3.569	0.000	0.003	53.843	0.137	0.026	0.000	0.043	0.106	96.669
19	41.172	0.048	3.568	0.000	0.004	54.567	0.066	0.003	0.000	0.033	0.126	98.084
20	40.574	0.000	3.576	0.000	0.003	54.442	0.038	0.068	0.000	0.077	0.152	97.423
21	41.397	0.017	3.517	0.000	0.004	54.695	0.046	0.019	0.000	0.011	0.089	98.313
22	40.572	0.048	3.470	0.168	0.004	54.443	0.056	0.028	0.000	0.054	0.090	97.471

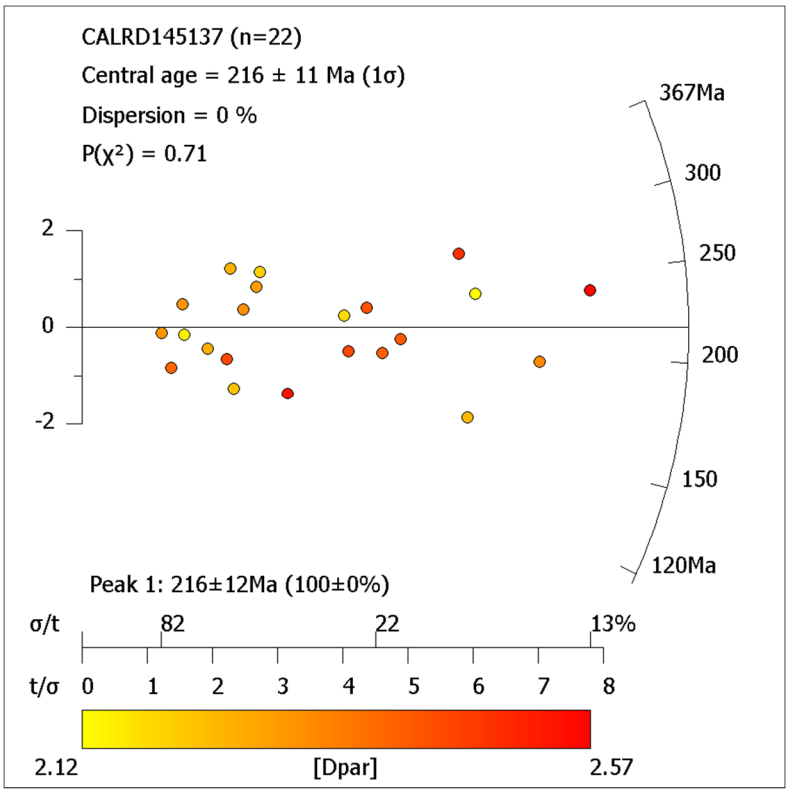

SAMPLE: CALRD145139

Age: Archean
Geological unit: Cadillac Group
Type: Greywacke

Coordinates - UTM83-17

Easting	689535.97
Northing	5346545.46
Elevation (N.M.M.)	-2602.89

present-day temperature 45˚C

GRAIN_DATA

Number of grains	20
Number of Dpars	80

Grain#	Ns	Ni	# square	MDpar	MDprp	U (ppm)
1	53	65	12	2.629	0.947	69
2	29	39	20	2.553	0.987	25
3	123	97	20	2.732	1.084	62
4	28	35	12	2.397	1.063	37
5	40	34	12	2.639	1.123	36
6	55	52	14	2.639	1.056	47
7	12	10	12	2.342	1.017	11
8	25	19	12	2.655	1.024	20
9	50	51	15	2.369	1.027	43
10	57	72	24	2.625	1.011	38
11	90	108	40	2.342	1.003	34
12	41	65	25	2.538	1.003	33
13	10	19	16	2.355	0.991	15
14	50	83	20	2.631	1.156	53
15	16	25	14	2.721	1.153	23
16	39	41	20	2.599	1.12	26
17	44	50	12	2.664	0.988	53
18	36	45	9	2.701	1.018	64
19	36	34	15	2.41	1.138	29
20	84	106	15	2.649	1.034	90

LENGTH_DATA

Number_of_lens	32
Number_of_dpar	96

#	Len	Type	MDpar	MDprp	NDpar	Angle with C-axis
1	11.577	T	2.769	1.001	4	72.84
2	11.866	T	2.769	1.001	0	54.741
3	14.633	T	2.607	1.015	4	60.787
4	14.019	T	2.607	1.015	0	80.44
5	13.649	T	2.769	1.236	4	66.729
6	9.674	T	2.769	1.236	0	79.48
7	12.128	T	2.57	1.071	4	74.963
8	10.241	T	2.57	1.071	0	62.791
9	13.163	T	2.617	0.901	4	58.748
10	13.169	T	2.798	0.954	4	66.663
11	7.194	T	2.537	1.031	4	60.44
12	12.567	T	2.451	1.104	4	66.563
13	8.726	T	2.569	0.889	4	79.873
14	12.003	T	2.584	1.169	4	66.412
15	3.53	T	2.833	1.091	4	84.286
16	8.809	T	2.505	1.057	4	86.638
17	11.051	T	2.505	1.057	0	64.417
18	11.393	T	2.505	1.057	0	70.535
19	11.131	T	2.425	1.116	4	62.902
20	11.753	T	2.438	1.012	4	54.698
21	12.409	T	2.44	0.828	4	47.862
22	10.61	T	2.424	1.201	4	35.911
23	9.346	T	2.424	1.201	0	73.417
24	6.13	T	2.522	0.948	4	61.606
25	5.246	T	2.711	0.974	4	31.698
26	5.088	T	2.707	1.116	4	65.861
27	3.152	T	2.707	1.116	0	80.257
28	9.251	T	2.582	1.163	4	59.834
29	9.328	T	2.39	1.076	4	51.675
30	4.146	T	2.481	1.189	4	69.084
31	12.94	T	2.351	1.057	4	64.884
32	11.59	T	2.252	1.15	4	64.196

TRACK_LENGTH_SUMMARY

Number	0	32	0	32	0	0
Mean_Len	-1	10.047	-1	10.047	-1	-1
SE_Mean	0	0.563	0	0.563	0	0
SD_Dist	0	3.183	0	3.183	0	0
Skewness	0	-0.824	0	-0.824	0	0
Kurtosis	0	-0.268	0	-0.268	0	0

MICROPROBE DATA

MASS PERCENT

Grain No.	P2O5	La2O3	F	SiO2	Cl	CaO	Ce2O3	Na2O	SrO	FeO	MnO	Total
1	42.214	0.038	3.311	0.000	0.008	54.598	0.043	0.047	0.000	0.128	0.189	99.180
2	42.149	0.095	3.613	0.000	0.001	54.780	0.084	0.028	0.000	0.314	0.225	99.768
3	41.364	0.006	3.431	0.000	0.000	55.753	0.056	0.022	0.000	0.098	0.185	99.470
4	41.853	0.000	3.188	0.000	0.001	55.016	0.069	0.024	0.000	0.219	0.186	99.214
5	42.618	0.000	3.433	0.000	0.002	55.333	0.064	0.005	0.000	0.059	0.142	100.211
6	42.085	0.000	3.446	0.000	0.000	54.608	0.053	0.041	0.000	0.298	0.203	99.283
7	41.956	0.000	3.243	0.000	0.000	55.399	0.023	0.048	0.000	0.073	0.157	99.534
8	41.055	0.000	3.598	0.000	0.000	54.310	0.000	0.026	0.000	1.120	0.140	98.734
9	41.530	0.023	3.176	0.000	0.000	54.839	0.038	0.025	0.000	0.098	0.141	98.533
10	42.248	0.000	3.179	0.000	0.019	55.509	0.003	0.053	0.000	0.121	0.191	99.980
11	41.959	0.000	3.183	0.000	0.000	55.376	0.000	0.033	0.000	0.108	0.143	99.462
12	41.751	0.000	3.398	0.000	0.001	55.240	0.053	0.040	0.000	0.206	0.199	99.457
13	42.571	0.012	3.190	0.000	0.004	54.812	0.018	0.029	0.000	0.126	0.223	99.641
14	41.742	0.059	3.540	0.031	0.007	55.213	0.076	0.039	0.000	0.249	0.199	99.662
15	41.999	0.000	3.658	0.000	0.000	55.641	0.074	0.024	0.000	0.065	0.150	100.071
16	41.596	0.008	3.289	0.000	0.004	55.079	0.056	0.035	0.000	0.290	0.193	99.164
17	42.411	0.113	3.400	0.000	0.000	54.423	0.000	0.033	0.000	0.125	0.161	99.234
18	41.949	0.035	3.465	0.000	0.004	54.431	0.041	0.020	0.000	0.042	0.170	98.697
19	42.182	0.000	3.345	0.000	0.005	55.304	0.000	0.038	0.000	0.191	0.178	99.834
20	41.990	0.041	3.470	0.000	0.001	55.442	0.000	0.054	0.000	0.096	0.157	99.790

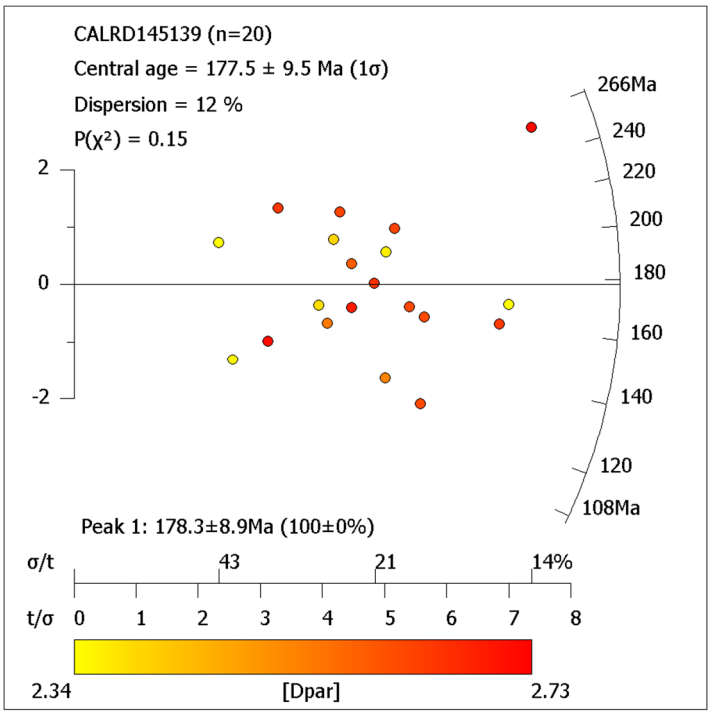

SAMPLE: CALRD145140

Age: Archean
Geological unit: Cadillac Group
Type: Greywacke

Coordinates - UTM83-17
Easting 689882.63
Northing 5346486.81
Elevation
(N.M.M.) -2968.90

present-day temperature 49˚C

GRAIN_DATA

Number of grains 20
Number of Dpars 80

Grain#	Ns	Ni	# square	MDpar	MDprp	U (ppm)
1	95	100	60	2.733	1.116	21
2	35	45	30	2.381	1.015	19
3	94	101	21	2.596	1.045	60
4	32	44	24	2.457	1.108	23
5	61	100	70	2.471	0.99	18
6	33	30	14	2.487	0.927	27
7	49	67	28	2.657	0.876	30
8	92	104	40	2.676	1.075	32
9	80	82	16	2.544	0.84	64
10	126	157	35	2.403	1.239	56
11	42	45	14	2.727	0.985	40
12	148	270	36	2.778	1.073	93
13	42	50	15	2.489	0.946	41
14	52	59	45	2.57	0.978	16
15	95	126	25	2.634	1.087	63
16	73	85	20	2.378	1.02	53
17	114	120	80	2.548	0.956	19
18	85	109	45	2.553	1.022	30
19	102	116	25	2.549	1.097	58
20	64	75	27	2.498	0.873	35

LENGTH_DATA

Number_of_lens	54
Number_of_dpar	120

#	Len	Type	MDpar	MDprp	NDpar	Angle with C-axis
1	14.354	T	2.742	1.157	4	71.816
2	11.223	T	2.742	1.157	0	-11.121
3	7.106	T	2.527	1.008	4	-85.236
4	7.18	T	2.311	1.005	4	-14.4
5	8.799	T	2.311	1.005	0	-22.62
6	6.977	T	2.468	1.141	4	-82.674
7	9.359	T	2.496	1.051	4	-28.657
8	8.945	T	2.496	1.051	0	5.412
9	11.674	T	2.506	1.053	4	-14.485
10	12.004	T	2.657	1.088	4	69.937
11	11.232	T	2.657	1.088	0	-57.144
12	10.693	T	2.657	1.088	0	86.82
13	13.905	T	2.582	0.915	0	80.34
14	6.625	T	2.582	0.915	4	-71.834
15	4.55	T	2.839	0.898	4	4.865
16	8.681	T	2.839	0.898	0	66.228
17	13.828	T	2.707	1.192	4	-36.793
18	11.497	T	2.707	1.192	0	40.865
19	8.213	T	2.349	1.266	4	62.549
20	12.7	T	2.52	0.956	4	-11.821
21	8.684	T	2.52	0.956	0	-10.814
22	11.146	T	2.52	0.956	0	-1.975
23	7.374	T	2.52	0.956	0	-68.629
24	11.578	T	2.504	1.012	4	53.696
25	11.782	T	2.562	1.159	4	-35.538
26	9.337	T	2.562	1.159	0	77.784
27	11.022	T	2.611	0.81	4	-31.675
28	11.154	T	2.611	0.81	0	8.556
29	8.948	T	2.62	1.256	4	-74.141
30	7.43	T	2.62	1.256	0	62.418
31	11.59	T	2.706	1.112	4	56.174
32	11.982	T	2.604	1.055	4	42.306
33	13.926	T	2.579	1.114	4	-45.285
34	12.085	T	2.579	1.114	0	-69.027
35	13.447	T	2.754	1.108	4	-60.781
36	8.117	T	2.754	1.108	0	-78.959
37	13.416	T	2.754	1.108	0	-55.408
38	12.004	T	2.397	1.034	4	59.349
39	9.574	T	2.397	1.034	0	56.952
40	12.373	T	2.397	1.034	0	60.199
41	10.682	T	2.397	1.034	0	-5.29
42	11.074	T	2.45	0.92	4	-62.103
43	10.049	T	2.45	0.92	0	-58.465
44	11.806	T	2.719	1.031	4	-11.991
45	9.283	T	2.48	1.138	4	73.974
46	13.337	T	2.48	1.138	0	-72.773
47	9.879	T	2.68	0.93	4	-78.111
48	7.245	T	2.621	0.924	4	57.171
49	5.591	T	2.749	1.067	4	-55.491
50	12.514	T	2.587	1.09	4	-46.828
51	6.549	T	2.587	1.09	0	-36.158
52	9.686	T	2.61	1.004	4	57.068
53	10.396	T	2.517	1.052	4	76.097
54	5.154	T	2.517	1.052	0	59.421

TRACK_LENGTH_SUMMARY

Number	0	54	0	54	0	0
Mean_Len	-1	10.217	-1	10.217	-1	-1
SE_Mean	0	0.328	0	0.328	0	0
SD_Dist	0	2.435	0	2.435	0	0
Skewness	0	-0.394	0	-0.394	0	0
Kurtosis	0	-0.604	0	-0.604	0	0

MICROPROBE DATA

MASS PERCENT

Grain No.	P2O5	La2O3	F	SiO2	Cl	CaO	Ce2O3	Na2O	SrO	FeO	MnO	Total
1	41.174	0.003	3.347	0.000	0.035	53.184	0.065	0.051	0.000	0.095	0.176	96.713
2	41.186	0.049	3.267	0.000	0.003	54.367	0.000	0.047	0.000	0.195	0.155	97.892
3	40.944	0.075	2.733	0.055	0.002	54.492	0.000	0.103	0.000	0.338	0.116	97.707
4	41.093	0.000	3.207	0.000	0.119	55.116	0.060	0.052	0.000	0.153	0.066	98.489
5	41.088	0.023	3.121	0.000	0.000	54.111	0.073	0.041	0.000	0.179	0.131	97.453
6	41.127	0.011	3.461	0.000	0.020	54.189	0.120	0.079	0.000	0.044	0.137	97.726
7	41.709	0.000	3.161	0.000	0.005	54.163	0.000	0.039	0.000	0.094	0.168	98.007
8	41.011	0.030	3.278	0.000	0.000	53.692	0.023	0.044	0.000	0.101	0.131	96.930
9	41.258	0.016	3.502	0.000	0.289	54.109	0.003	0.024	0.000	0.012	0.160	97.833
10	41.208	0.044	3.366	0.000	0.000	54.231	0.000	0.026	0.000	0.207	0.149	97.814
11	41.245	0.000	3.277	0.036	0.003	54.505	0.107	0.037	0.000	0.070	0.099	97.998
12	41.168	0.000	3.428	0.000	0.000	54.516	0.031	0.041	0.000	0.065	0.156	97.962
13	41.157	0.058	3.374	0.061	0.000	54.025	0.078	0.029	0.000	0.247	0.131	97.739
14	41.286	0.008	3.262	0.000	0.009	53.664	0.078	0.051	0.000	0.076	0.138	97.197
15	40.278	0.016	3.410	0.163	0.000	53.360	0.031	0.050	0.000	0.216	0.151	96.239
16	41.669	0.000	3.414	0.000	0.020	53.881	0.094	0.042	0.000	0.065	0.097	97.840
17	40.972	0.000	3.417	0.000	0.000	53.092	0.000	0.049	0.000	0.019	0.163	96.273
18	40.479	0.000	2.920	0.000	0.000	54.383	0.010	0.030	0.000	0.062	0.142	96.797
19	41.881	0.016	3.409	0.000	0.006	54.365	0.047	0.031	0.000	0.088	0.160	98.567
20	40.992	0.047	3.193	0.000	0.000	54.215	0.000	0.049	0.000	0.134	0.144	97.430

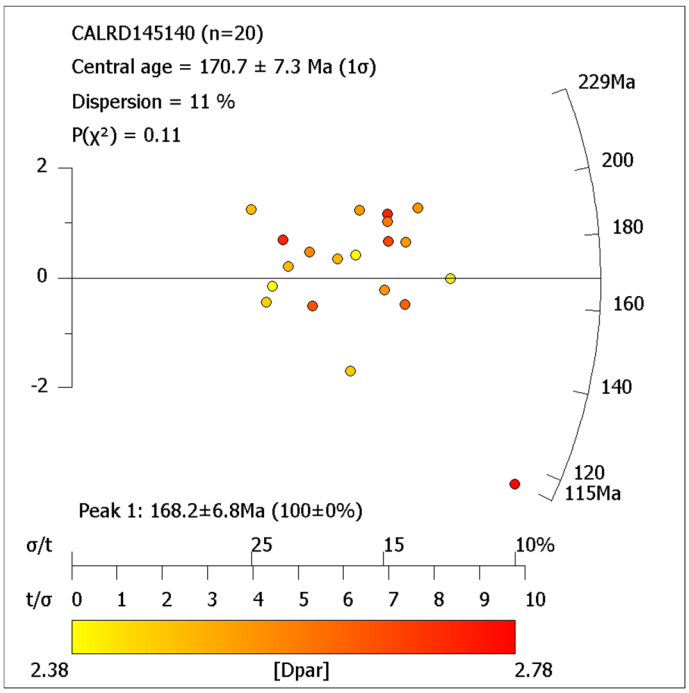

SAMPLE: CALRD145141

Age: Archean
Geological unit: Cadillac Group
Type: greywacke

Coordinates - UTM83-17
Easting 689891.29
Northing 5346353.45
Elevation (N.M.M.) -3361.99

present-day temperature

GRAIN_DATA

Number of grains 20
Number of Dpars 85

Grain#	Ns	Ni	# square	MDpar	MDprp	U (ppm)	Age (Ma)	-95%	95%
1	50	61	18	2.485	1.093	41	176	-55.7	81
2	9	13	15	2.537	1.037	11	148.9	-86	201
3	76	104	21	2.579	0.976	60	157.1	-41.1	55.3
4	85	139	36	2.437	1.055	47	131.7	-31.9	42
5	12	13	21	2.632	0.949	8	197.8	-108	235
6	39	46	20	2.551	1.158	28	181.9	-64	97.9
7	10	12	12	2.315	1.035	12	178.8	-102	235
8	109	193	54	2.355	1.034	44	121.7	-26.3	33.4
9	26	42	32	2.385	1.081	16	133.3	-52.3	85.4
10	7	14	20	2.335	0.973	9	107.9	-65	161
11	121	151	100	2.504	1.072	18	172.1	-37.6	47.9
12	14	16	20	2.512	1.201	10	187.7	-96.9	197
13	43	51	12	2.517	1.104	52	180.9	-61.1	91.7
14	84	129	24	2.36	1.02	66	140.2	-34.5	45.6
15	17	28	18	2.546	0.98	19	130.8	-59.9	110
16	27	34	15	2.585	1.112	28	170.5	-68.4	113
17	68	106	60	2.582	1.158	22	138.1	-37	50.4
18	5	4	21	2.487	0.99	2	266.4	-196	699
19	67	89	64	2.428	1.121	17	161.8	-44.8	61.6
20	17	23	25	2.553	0.915	11	158.9	-74.8	140
21	48	85	60	2.358	1.099	17	121.7	-37	52.9

LENGTH_DATA

Number_of_lens	62
Number_of_dpar	165

#	Len	Type	MDpar	MDprp	NDpar	Angle with C-axis
1	14.467	T	2.604	1.002	4	32.812
2	12.066	T	2.486	1.005	4	67.129
3	10.157	T	2.486	1.005	0	84.151
4	5.765	T	2.681	1.105	4	88.567
5	9.639	T	2.538	1.072	4	59.406
6	11.987	T	2.538	1.072	0	56.235
7	11.959	T	2.638	1.19	4	63.173
8	10.891	T	2.638	1.19	0	63.15
9	10.407	T	2.391	1.161	4	74.015
10	10.478	T	2.594	0.991	4	88.873
11	5.368	T	2.5	0.922	4	78.01
12	9.792	T	2.5	0.922	0	67.174
13	5.8	T	2.5	0.922	0	75.708
14	10.73	T	2.5	0.922	0	57.127
15	11.536	T	2.416	0.98	4	67.783
16	7.519	T	2.428	1.002	4	83.404
17	10.16	T	2.558	0.973	4	62.666
18	11.364	T	2.619	1.179	4	73.198
19	13.216	T	2.619	1.179	0	40.536
20	6.547	T	2.217	1.003	4	82.992
21	12.447	T	2.701	1.087	4	76.396
22	11.472	T	2.44	1.066	4	69.517
23	12.223	T	2.44	1.066	0	17.013
24	7.896	T	2.335	0.985	4	84.408
25	5.831	T	2.61	1.147	4	49.467
26	13.551	T	2.427	1.053	4	75.43
27	13.179	T	2.536	1.008	4	53.68
28	12.761	T	2.536	1.008	0	64.677
29	13.894	T	2.536	1.008	0	47.961
30	7.993	T	2.46	1.174	4	53.628
31	12.502	T	2.309	1.167	4	60.346
32	8.795	T	2.544	1.127	4	67.956
33	12.161	T	2.545	1.027	4	21.478
34	12.924	T	2.727	1.123	4	50.663
35	4.868	T	2.727	1.123	0	85.498
36	9.834	T	2.603	1.077	4	59.952
37	11.591	T	2.603	1.077	0	62.277
38	10.774	T	2.459	1.089	4	76.98
39	10.051	T	2.459	1.089	0	39.333
40	11.962	T	2.392	0.98	4	75.417
41	11.558	T	2.431	1.036	4	48.325
42	13.599	T	2.431	1.036	0	43.442
43	7.214	T	2.702	0.865	4	59.82
44	6.433	T	2.702	0.865	0	36.963
45	10.856	T	2.515	1.078	4	73.443
46	8.158	T	2.515	1.078	0	79.674
47	11.216	T	2.376	0.936	4	66.438
48	11.988	T	2.376	0.936	0	75.906
49	10.302	T	2.384	1.023	4	66.473
50	8.196	T	2.384	1.023	0	79.799
51	7.484	T	2.615	1.144	4	75.69
52	9.14	T	2.539	1.076	4	75.78
53	5.802	T	2.539	1.076	0	61.494
54	9.787	T	2.405	0.957	4	69.481
55	12.232	T	2.405	0.957	0	71.602
56	9.364	T	2.397	0.937	4	85.232
57	13.375	T	2.447	0.945	4	68.392
58	11.544	T	2.447	0.945	0	64.779
59	12.188	T	2.35	0.988	5	31.597
60	8.562	T	2.634	0.934	4	60.238
61	9.783	T	2.322	1.023	4	47.39
62	14.006	T	2.602	1.116	4	39.696

TRACK_LENGTH_SUMMARY

Number	0	62	0	62	0	0
Mean_Len	-1	10.312	-1	10.312	-1	-1
SE_Mean	0	0.314	0	0.314	0	0
SD_Dist	0	2.469	0	2.469	0	0
Skewness	0	-0.522	0	-0.522	0	0
Kurtosis	0	-0.606	0	-0.606	0	0

MASS PERCENT

Grain No.	P2O5	La2O3	F	SiO2	Cl	CaO	Ce2O3	Na2O	SrO	FeO	MnO	Total
1	41.253	0.083	3.430	0.000	0.001	54.079	0.000	0.037	0.000	0.075	0.180	97.694
2	41.768	0.155	3.559	0.000	0.025	54.509	0.038	0.034	0.000	0.047	0.088	98.718
3	41.354	0.007	3.434	0.000	0.030	54.264	0.020	0.015	0.000	0.094	0.065	97.830
4	42.193	0.043	3.335	0.000	0.002	54.422	0.018	0.038	0.000	0.168	0.092	98.907
5	41.700	0.000	3.549	0.000	0.240	55.208	0.031	0.035	0.000	0.040	0.078	99.333
6	42.064	0.000	3.232	0.000	0.017	54.366	0.000	0.037	0.000	0.066	0.110	98.527
7	41.107	0.000	3.599	0.000	0.000	54.104	0.028	0.035	0.000	0.044	0.075	97.477
8	41.733	0.000	3.425	0.000	0.001	54.959	0.058	0.053	0.000	0.071	0.075	98.933
9	41.443	0.000	3.259	0.000	0.001	54.694	0.015	0.018	0.000	0.028	0.097	98.183
10	42.263	0.000	3.365	0.000	0.019	54.678	0.036	0.042	0.000	0.040	0.079	99.101
11	42.091	0.000	3.344	0.000	0.009	54.631	0.081	0.045	0.000	0.055	0.135	98.981
12	42.002	0.023	3.151	0.000	0.009	54.423	0.084	0.037	0.000	0.032	0.087	98.519
13	41.538	0.007	3.206	0.000	0.004	54.254	0.018	0.011	0.000	0.184	0.107	97.978
14	41.590	0.012	3.411	0.000	0.004	54.401	0.086	0.041	0.000	0.039	0.127	98.274
15	40.865	0.000	3.282	0.000	0.001	55.043	0.053	0.048	0.000	0.044	0.126	98.080
16	41.003	0.000	3.419	0.000	0.000	54.391	0.041	0.047	0.000	0.090	0.146	97.697
17	41.055	0.000	3.220	0.000	0.000	53.766	0.056	0.053	0.000	0.071	0.102	96.967
18	40.941	0.008	3.524	0.000	0.017	55.223	0.005	0.029	0.000	0.031	0.030	98.320
19	41.906	0.075	3.575	0.000	0.003	54.271	0.000	0.011	0.000	0.043	0.099	98.477
20	41.130	0.000	3.467	0.000	0.014	54.877	0.081	0.032	0.000	0.080	0.081	98.299
21	41.908	0.000	3.420	0.000	0.006	54.746	0.005	0.020	0.000	0.169	0.071	98.904